Phase Relations of Peralkaline Silicic Magmas and Petrogenetic Implications

Bruno Scaillet, Ray Macdonald

JOURNAL OF PETROLOGY | VOLUME 42 | NUMBER 4 | PAGES 825–845 | 2001

Phase Relations of Peralkaline Silicic Magmas and Petrogenetic Implications

BRUNO SCAILLET[1]* AND RAY MACDONALD[2]

[1]INSTITUT DES SCIENCES DE LA TERRE D'ORLÉANS, CNRS, 1A RUE DE LA FÉROLLERIE, 45071, ORLÉANS CEDEX 2, FRANCE

[2]ENVIRONMENTAL SCIENCES DIVISION, IENS, LANCASTER UNIVERSITY, LANCASTER LA1 4YQ, UK

RECEIVED NOVEMBER 29, 1999; REVISED TYPESCRIPT ACCEPTED JULY 21, 2000

The phase relationships of three peralkaline rhyolites from the Kenya Rift have been established at 150 and 50 MPa, at oxygen fugacities of NNO − 1·6 and NNO + 3·6 (log fO_2 relative to the Ni–NiO solid buffer), between 800 and 660°C and for melt H_2O contents ranging between saturation and nominally anhydrous. The stability fields of fayalite, sodic amphiboles, chevkinite and fluorite in natural hydrous silicic magmas are established. Additional phases include quartz, alkali feldspar, ferrohedenbergite, biotite, aegirine, titanite, montdorite and oxides. Ferrohedenbergite crystallization is restricted to the least peralkaline rock, together with fayalite; it is replaced at low melt water contents by ferrorichterite. Riebeckite–arfvedsonite appears only in the more peralkaline rocks, at temperatures below 750°C (dry) and below 670°C at H_2O saturation. Under oxidizing conditions, it breaks down to aegirine. In the more peralkaline rocks, biotite is restricted to temperatures below 700°C and conditions close to H_2O saturation. At 50 MPa, the tectosilicate liquidus temperatures are raised by 50–60°C, and that of amphibole by 30°C. Riebeckite–arfvedsonite stability extends down nearly to atmospheric pressure, as a result of its F-rich character. The solidi of all three rocks are depressed by 40–100°C compared with the solidus of the metaluminous granite system, as a result of the abundance of F and Cl. Low fO_2 lowers solidus temperatures by at least 30°C. Comparison with studies of metaluminous and peraluminous felsic magmas shows that plagioclase crystallization is suppressed as soon as the melt becomes peralkaline, whatever its CaO or volatile contents. In contrast, at 100 MPa and H_2O saturation, the liquidus temperatures of quartz and alkali feldspar are not significantly affected by changes in rock peralkalinity, showing that the incorporation of water in peralkaline melts diminishes the depression of liquidus temperatures in dry peralkaline silicic melts compared with dry metaluminous or peraluminous varieties. At 150 MPa, pre-eruptive melt H_2O contents range from 4 wt % in the least peralkaline rock to nearly 6 wt % in the two more peralkaline compositions, in broad agreement with previous melt inclusion data. The experimental results imply magmatic fO_2 at or below the fayalite–quartz–magnetite solid buffer, temperatures between 740 and 660°C, and melt evolution under near H_2O saturation conditions.

KEY WORDS: *peralkaline; rhyolite; phase equilibria*

INTRODUCTION

Since the field recognition of peralkaline igneous rocks by Foerstner (1881), much effort has been expended in the petrological, geochemical and experimental fields to understand their petrogenesis (e.g. Washington, 1913, 1914*a*, 1914*b*; Bowen, 1937; Zies, 1960; Carmichael, 1962; Carmichael & MacKenzie, 1963; Bailey & Schairer, 1964, 1966; Thompson & MacKenzie, 1967; Ewart *et al.*, 1968; Noble, 1968; Nicholls & Carmichael, 1969; Bailey & Macdonald, 1970; Gibson, 1972; Macdonald & Bailey, 1973; Bailey, 1974; Barberi *et al.*, 1974, 1975; Villari, 1974; Roux & Varet, 1975; Bailey & Cooper, 1978; Harris, 1983; Mahood, 1984; Mungall & Martin, 1995; Bohrson & Reid, 1997). For the vast majority of natural occurrences, peralkaline felsic rocks can be explained by fractional crystallization of mildly alkalic or transitional basalts at both low fH_2O and low fO_2 (e.g. Harris, 1983; Caroff *et al.*, 1993). Perhaps the best example of such a mechanism is the Boina volcanic rock suite in the Afar Rift, Ethiopia (Barberi *et al.*, 1975). Other studies have shown, however, that this simple

*Corresponding author. Telephone: 0033-2-38-25-53-40. Fax: 0033-2-38-63-64-88. E-mail: bscaille@cnrs-orleans.fr

petrogenetic scheme may not apply everywhere. Davies & Macdonald (1987), Macdonald *et al.* (1987) and Black *et al.* (1997), for instance, have conclusively shown, mainly on geochemical grounds, that the peralkaline rhyolites cropping out near Naivasha in the Kenyan Rift Valley (the Greater Olkaria Volcanic Complex, GOVC) cannot be the daughter magmas of the associated basalts, and they proposed an origin by partial melting of the crust triggered by alkali-bearing volatiles. Mahood *et al.* (1990) proposed that pantellerite rhyolites at the type locality of Pantelleria are the product of a two-step process, whereby partial melting of alkali gabbros yields trachyte melts whose subsequent fractionation ends in the strongly peralkaline rhyolites [but see Civetta *et al.* (1998)].

All studies up to 1988 agreed as to the dry, or at least the very H_2O-poor, character of peralkaline rhyolites, in particular when compared with their metaluminous equivalents. The reasons for believing so (Bailey & Macdonald, 1987) include the nearly anhydrous state of all peralkaline obsidians, their high Cl content, thought to be incompatible with the exsolution of a hydrous vapour phase, and the fact that phase equilibrium experiments performed under dry conditions better reproduce the crystallization sequence in the rocks than those under wet conditions (Bailey, 1974). Another rarely considered factor is that peralkalinity is accompanied by a significant fall in liquidus temperatures relative to metaluminous rhyolites. This was apparent in the pioneering studies of Schairer & Bowen (1955, 1956), who worked out the phase relationships in the dry synthetic Na_2O–Al_2O_3–SiO_2 and K_2O–Al_2O_3–SiO_2 ternaries and found eutectic temperatures as low as 740°C at 1 bar on the peralkaline sides. Addition of iron to the Na_2O–Al_2O_3–SiO_2 system does not change the trend of falling temperatures (Bailey & Schairer, 1966), with even lower eutectic temperatures, around 728°C, in the SiO_2-oversaturated field of the Na_2O–Al_2O_3–SiO_2–Fe_2O_3 system. The implication is that there are no thermal limitations to generating dry silicic peralkaline melts by direct melting of crust under dry conditions (given a suitable protolith), a conclusion in sharp contrast to metaluminous or peraluminous systems where dry melting requires temperatures of $\sim$1000°C (Bowen, 1937), i.e. temperatures unlikely to be reached in the crust, even in extensional tectonic settings.

Melt inclusion studies of peralkaline rhyolites, however, have found significant amounts of dissolved H_2O (1·4–5 wt %, Ascension: Harris, 1986; Pantelleria: Kovalenko *et al.*, 1988; Lowenstern & Mahood, 1991; Fantale, Ethiopia: Webster *et al.*, 1993; GOVC, Kenya: Wilding *et al.*, 1993; Mayor Island, New Zealand: Barclay *et al.*, 1996). Although this conflicts with previously available phase equilibrium constraints (Bailey, 1974), it is worth stressing that our knowledge of the physico-chemical conditions of the evolution of peralkaline silicic magmas is still surprisingly poor. For instance, because of the scarcity of coexisting Fe–Ti oxide minerals in peralkaline rocks, pre-eruptive temperatures are poorly constrained. The few quantitative estimates available (Carmichael, 1967, 1991; Bizouard *et al.*, 1980; Mahood, 1981; Wolff & Wright, 1981; Conrad, 1984; Novak & Mahood, 1986; Crisp & Spera, 1987; Jørgensen, 1987; Ghiorso & Sack 1991) indicate pre-eruptive temperatures in the range 700–950°C at fO_2 generally close to the fayalite–magnetite–quartz buffer (FMQ).

Available experimental work is of little use in constraining the pre-eruptive conditions of peralkaline magmas (Webster *et al.*, 1993). Most studies have been performed in synthetic systems under either dry (Bailey & Schairer, 1966) or water-saturated conditions (Carmichael & MacKenzie, 1963; Thompson & MacKenzie, 1967). The same problem applies to the few experimental studies on natural peralkaline rhyolites (Bailey & Cooper, 1978). In addition, in none of these studies was the fO_2 carefully controlled. Experiments at H_2O saturation have all been performed under very oxidizing conditions which seriously contrast with the rock record (Carmichael, 1962; Nicholls & Carmichael, 1969; Sutherland, 1974). Thus, the phase equilibria of peralkaline magmas are poorly known compared with their metaluminous or peraluminous silicic counterparts (e.g. Clemens & Wall, 1981; Clemens *et al.*, 1986; Webster *et al.*, 1987; Conrad *et al.*, 1988; Scaillet *et al.*, 1995; Martel *et al.*, 1998, 1999; Dall'Agnol *et al.*, 1999; Scaillet & Evans, 1999), which seriously hinders any attempt at constraining their evolution. This work intends to fill this gap by determining the phase relationships of three natural peralkaline rhyolites under controlled fO_2 and fH_2O conditions. Although our main goal is to provide quantitative estimates of pre-eruptive conditions, the comprehensive phase equilibrium data provided should prove useful in determining the pre-eruptive conditions of other mildly to moderately peralkaline silicic rocks.

ROCKS STUDIED

The three natural rhyolites used come from the Greater Olkaria Volcanic Complex in the Naivasha area of the Kenyan Rift Valley, where the geology is well known (Clarke *et al.*, 1990) and where there has been extensive petrological and geochemical work (Bailey & Macdonald, 1987; Davies & Macdonald, 1987; Macdonald *et al.*, 1987; Black *et al.*, 1997; Marshall *et al.*, 1998). The three rocks are phenocryst-poor obsidians; bulk compositions are listed in Table 1. They are comendites in the classification scheme of Macdonald (1974), with agpaitic indices [(Na + K)/Al, in moles] ranging from 1·05 to 1·36. They represent the two extremes of the geochemical

range displayed by the comendite suite at Olkaria (Macdonald *et al.*, 1987). Sample ND 002 is only marginally peralkaline and has <5% (volume) phenocrysts of alkali feldspar, clinopyroxene, fayalite, magnetite, zircon, apatite and chevkinite. The glassy matrix has the same agpaitic index as the bulk rock (Table 1). Sample BL 575 is the most peralkaline specimen (NK/A = 1·36). It has 5% phenocrysts of alkali feldspar, quartz, riebeckite–arfvedsonite, aenigmatite, biotite, ilmenite and chevkinite. BL 575 contains some spherulites with a radial arrangement of riebeckite laths and aggregates of quartz and alkali feldspar. Microphenocrysts of riebeckite–arfvedsonite also occur in the matrix glass. Sample SMN 49 is chemically similar to BL 575, being only slightly more SiO_2 rich and less peralkaline (Table 1). Its phenocryst assemblage differs from that of BL 575 in the occurrence of fluorite (Marshall *et al.*, 1998) and the absence of riebeckite and aenigmatite. Also, it has lower Fe_2O_3/FeO than BL 575 (Table 1). In both BL 575 and SMN 49, the matrix glass is slightly more peralkaline than the bulk rock (Table 1). For all three samples, microprobe analyses of the matrix glass yield totals close to 100%, implying water contents <1 wt %. This is confirmed by Fourier transform IR spectroscopy (FTIR) analyses carried out on sample ND 002, whose matrix glass has 1800 ppm dissolved H_2O (Wilding *et al.*, 1993). FTIR analyses performed by Wilding *et al.* (1993) on samples belonging to the same suite as BL 575 and SMN 49 yielded similar results.

EXPERIMENTAL AND ANALYTICAL TECHNIQUES

Preparation of charges

Hydrothermal experiments were performed using rock powders as starting material. Therefore, given the near-aphyric character of the natural rhyolites, most experiments in this study were of crystallization type (e.g. Clemens & Wall, 1981; Pichavant, 1987; Conrad *et al.*, 1988; Scaillet *et al.*, 1995; Martel *et al.*, 1998; Dall'Agnol *et al.*, 1999; Scaillet & Evans, 1999). Charges consisted of Au capsules (length 1·5–1·2 cm, thickness 0·02 cm, inner diameter 0·29–0·27 cm), first loaded with deionized water, then with silver oxalate as a source of CO_2 for H_2O-undersaturated experiments, and finally with the rock powder. Fluids of various H_2O/CO_2 ratio were used as a practical means of varying the water activity (aH_2O) at any given temperature (T) and pressure (P) but also because geological evidence points to a role for CO_2 in the petrogenesis of felsic peralkaline magmas in the Kenya rift (Bailey & Macdonald, 1987; Macdonald *et al.*, 1993). The weight proportion of $H_2O + CO_2$ [i.e. $(H_2O + CO_2)/(H_2O + CO_2 +$ silicate)] in most charges was maintained in the range 7–10 except for charge numbers 1–7, in which this parameter was around four (in the following, XH_2O_{in} refers to the initial mole fraction of H_2O in the fluid phase loaded to the capsule). A single series of experiments was also performed with only H_2O added in amounts below those required for saturation. Nominally dry charges were also prepared simply by loading the rock powder into Au capsules. These charges contain in fact 0·2–0·4 wt % water, owing to the presence of residual H_2O in the matrix glass and adsorbed water. Upon loading, capsules were sealed by arc-welding, immersed in a 120°C oil bath, and then weighed to check for leaks. After completion of an experiment, capsules were reweighed to ensure closed-system behaviour at P and T.

Equipment

All experiments were performed in standard cold-seal pressure vessels with or without semi-permeable H_2 membranes (respectively designed CSPV-H_2 and CSPV). Total pressure is known to within 2 MPa. Temperatures were continuously recorded by external unsheathed type-K thermocouples and are known to ± 8°C. Experiments performed with an H_2 membrane were terminated by removing the vessel from the furnace and allowing it to cool in air. To minimize exsolution, most experiments (charges with numbers higher than 12) were terminated using a small ventilator to accelerate cooling and by maintaining isobaric conditions down to 150°C. Experiments performed without H_2 membranes at 150 MPa were drop quenched. For each composition, phase equilibria were established at two pressures, 50 and 150 MPa, and under two contrasting redox conditions, in the temperature range 660–800°C. Run durations varied according to temperature, between 7 days at around 800°C and 51 days at or below 700°C. A total of 158 phase equilibrium experiments was performed.

fH_2 control

Two types of vessels were used to perform either reduced (CSPV-H_2) or oxidized (CSPV) experiments. In the former, the hydrogen fugacity (fH_2) was read continuously via H_2 membranes connected to a transducer with an uncertainty of 0·01 MPa (Scaillet *et al.*, 1992; Schmidt *et al.*, 1995; Scaillet & Evans, 1999). Under oxidizing conditions the fH_2 of the vessel was determined by using the dependence of the ferric/ferrous ratio of the three bulk compositions on fH_2. This relationship was calibrated by annealing the rock powders at 150 MPa, 800°C, H_2O saturation and various fH_2, as monitored with H_2 membranes. Volumetric titration of the ferrous iron content of the run products yields the relationship between FeO content and fH_2 specific to each composition. Subsequent

Table 1: Bulk-rock and matrix glass compositions (wt %)

Sample no.:	ND 002		BL 575		SMN 49	
	bulk[1]	matrix glass	bulk[2]	matrix glass	bulk[2]	matrix glass
n:[3]		6		5		6
SiO_2	75·2	75·92 (21)[4]	72·64	73·24 (15)	74·17	73·47 (43)
TiO_2	0·17	0·11 (6)	0·18	0·14 (2)	0·17	0·12 (5)
Al_2O_3	12·11	11·99 (12)	10·30	10·25 (16)	10·89	10·49 (14)
Fe_2O_3	0·83	—	1·39	—	1·98	—
FeO	1·06	—	2·75	—	2·21 (2)	—
FeO_{tot}	1·81	1·70 (16)	4·00	4·09 (22)	3·98	3·82 (23)
MnO	0·04	0·02 (3)	0·06	0·05 (5)	0·06	0·10 (8)
MgO	0·07	0·03 (3)	0·04	0·01 (1)	0·00	0·02 (1)
CaO	0·44	0·34 (3)	0·10	0·05 (4)	0·29	0·06 (4)
Na_2O	4·59	4·43 (16)	5·68	5·64 (10)	5·81	5·68 (11)
K_2O	4·73	4·85 (8)	4·35	4·89 (7)	4·34	4·68 (20)
F	0·37	0·38 (8)	1·00	1·11 (11)	1·00	1·03 (11)
Cl	0·22	0·17 (2)	0·50	0·50 (5)	0·50	0·50 (3)
LOI	0·06	—	0·79	—	—	—
Total	99·80	98·78	98·59	98·43	100·15	99·73
Sr	6	—	1	—	—	—
Rb	290	—	668	—	741	—
Zr	439	—	2198	—	2666	—
NK/A (mole)	1·05	1·05	1·36	1·42	1·31	1·37
$FeO/FeO + Fe_2O_3$ (wt %)	0·56	—	0·66	—	0·53	—

[1]From Macdonald *et al.* (1987).
[2]BL 575 and SMN 49 bulk analyses from Black *et al.* (1997) and Marshall *et al.* (1998), respectively, except for FeO determined by wet chemistry in this study, and for F and Cl, determined by EMPA of corresponding supraliquidus glasses.
[3]Number of analyses.
[4]Numbers in parentheses indicate 1 SD of replicate analyses in terms of smallest units cited.

determination of the ferrous content of H_2O-saturated charges around 800°C thus gives the fH_2 of that run. The fH_2 varies among the vessels, between 0·011 and 0·004 MPa; these values correspond to fO_2 3·6–4·4 log units above that of the Ni–NiO solid buffer (NNO + 3·6 to NNO + 4·4) at H_2O saturation. The fH_2 obtained at that temperature for a given vessel was considered constant for that vessel and used for subsequent fO_2 calculations at lower temperatures. The fO_2 of two vessels used without an H_2 membrane was also measured using solid NiPd sensors (Taylor *et al.*, 1992; Pownceby & O'Neill, 1994). Values of NNO + 3 to NNO + 5·1 were obtained, straddling the haematite–magnetite equilibrium.

fO_2 determination

The fO_2 of fluid-saturated charges was calculated using the equation (see Scaillet & Evans, 1999)

$$\log fO_2(\text{charge}) = \log fO_2(H_2O \text{ saturation}) - 2\log(XH_2O_{in}). \quad (1)$$

For experiments performed at high fH_2, the vast majority of fO_2 values fall in the range NNO –1 to NNO − 2, with an average at NNO − 1·67 ± 0·4. For experiments performed at low fH_2, most of the calculated fO_2 are in the range NNO + 3 to NNO + 4, with an average at NNO + 3·63 ± 0·44. Thus, for simplicity, average values of NNO − 1·6 and NNO + 3·6 are used in the following to characterize runs performed under reduced and oxidized conditions, respectively. At XH_2O values <0·3, however, the fO_2 starts to decrease significantly relative to that at H_2O saturation, by several orders of magnitude for extremely H_2O-poor charges (see Webster *et al.*, 1987). For nominally dry charges the amount of H_2O present in the fluid phase, if any, depends on the amount of both adsorbed and dissolved H_2O of the rock powder, which can vary between charges and cannot be evaluated rigorously. For instance, the fO_2

of nominally dry charges calculated using equation (1) assuming a fluid phase composition of $XH_2O = 0{\cdot}01$ is around NNO for dry charges at low fH_2, or 5 log units below it (NNO − 5) for dry charges at fH_2 = 20–30 bar. The same calculation with $XH_2O = 0{\cdot}1$ yields fO_2 of NNO + 2 to NNO − 3, respectively. This shows that, if extremely dry, runs performed at low fH_2 may have fO_2 values approaching those of H_2O-saturated charges at high fH_2.

For experiments carried out with CSPV-H_2 at H_2O saturation, the calculated fO_2 values are accurate to within 0·03 log units whereas those calculated for H_2O-undersaturated charges must be seen as maxima, as equation (1) overestimates the abundance of H_2O in the fluid and neglects the departure from ideality of H_2O–CO_2 fluid. For experiments performed in CSPV, the uncertainty of fO_2 is larger. In runs for which fH_2 has been determined (runs at ∼800°C), we evaluate the uncertainty to be around ±0·6 unit log. For runs performed in CSPV at lower temperatures, the error on our calculated fO_2 can be much larger, possibly approaching 1 log unit. We consider, however, that all the runs performed in CSPV have their fO_2 within the range NNO + 3 to NNO + 5 (excluding dry runs).

Analytical methods

Run products were characterized by polarized light microscopy, and by electron microprobe analysis (EMPA) and scanning electron microscopy (SEM). Analytical conditions for EMPA were accelerating voltage 15 kV, sample current 6 nA, counting time 10 s on peak for all elements and a focused beam for minerals. For glasses the beam was defocused to 5 μm. Na and K were analysed first and a ZAF correction procedure was applied. Na_2O migration under the probe beam was assessed using two sets of hydrous metaluminous and peralkaline (SMN 49) rhyolitic glass standards of known H_2O contents (Scaillet & Evans, 1999). At the beginning of each analytical session the two set of standards were analysed, the metaluminous being used for retrieving the Na_2O correction factor to be applied to composition ND 002, whereas the peralkaline set was used for calculating that specific to compositions BL 575 and SMN 49.

Melt H_2O contents (H_2O_{melt}) of drop-quenched glasses at 800 and 750°C were estimated using the by-difference method (Devine *et al.*, 1995) after correction for alkali migration. The precision of melt water contents is estimated to be 0·5 wt %. Experiments performed at lower temperatures display textural evidence of fluid exsolution during quench (sub-micrometric bubbles). The melt water content of these charges was estimated using the linear correlations between XH_2O_{in} and melt H_2O content obtained in drop-quenched charges at 800 and 750°C. These correlations were also used to calculate the melt water content of near-solidus charges in which the melt composition could not be microprobe analysed. For nominally anhydrous charges the melt H_2O content was calculated assuming perfectly incompatible behaviour for both H_2O and F during crystallization and using a bulk H_2O content for the three starting rock powders of 0·4 wt %.

Attainment of equilibrium

The successful crystallization of all the naturally occurring minerals apart from aenigmatite shows that no major nucleation problems were encountered in this study. At 800°C and 150 MPa, melting of the three H_2O-saturated samples was complete after 10 days. A few relict minerals were observed in some charges, mainly at temperatures below 750°C and at low XH_2O (Table 2), but their modal abundance is <0·5%, implying that the non-reactive part of the system was minimal. Experimental work performed in dry and H_2O-saturated peralkaline systems has shown that equilibrium conditions are attained during run durations of the order of a week (Carmichael & Mackenzie, 1963; Thompson & Mackenzie, 1967; Bailey *et al.*, 1974; Bailey & Cooper, 1978). In the present work, run duration was at least 10 days at 800°C and up to 8 weeks at temperatures below 700°C (Table 2). Previous researchers carrying out phase equilibrium experiments in metaluminous or peraluminous silicic systems have concluded that bulk equilibrium was reached for run durations similar to those applied in the present study (e.g. Clemens & Wall, 1981; Pichavant, 1987; Webster *et al.*, 1987; Holtz *et al.*, 1992; Scaillet *et al.*, 1995; Dall'Agnoll *et al.*, 1999). These lines of evidence argue for the attainment of near-equilibrium conditions in the experimental charges. Probe analyses show that in some runs, contamination by Ni from the vessel occurred, with the Ni content of ferromagnesian phases of a single charge varying in an erratic way from below detection up to several weight percent, suggesting that Ni was not instrumental in crystal growth. The FeO_{tot} content of glasses of supra-liquidus charges at low fO_2 is ∼6% lower than the starting bulk composition, showing that iron loss toward the Au capsules was minimal.

RESULTS

Phases and textures

Phases grown in our experiments are alkali feldspar, quartz, plagioclase, hedenbergite, magnetite, ilmenite, chevkinite, biotite, fayalite, zircon, fluorite, titanite, aegirine, ferrorichterite and riebeckite–arfvedsonite.

Table 2: Experimental results on Naivasha rhyolites

	P (bar)	*T* (°C)	P_{H_2} (bar)	Duration (h)	XH_2O_{in}[1]	log fO_2[2] (ΔNNO)	H_2O[3] (wt %)	Run products[4]
Sample ND 002								
150 MPa, reduced								
1	1540	797	26	255	1·00	−1·19	*4·87*	gl, vp
2	1556	788	25	378	0·90	−1·26	4·47	gl, vp
3	1556	788	25	378	0·79	−1·37	2·82	gl, vp, af, qtz, hd, ox
4	1505	788	23	354	0·72	−1·40	2·70	gl, vp, af, qtz, hd, fay, ox
5	1505	788	23	354	0·60	−1·56	—	gl, vp, af, qtz, hd, fay ox
6	1608	738	20	617	1·00	−1·05	4·56	gl, vp, hd, ox
7	1608	738	20	617	0·90	−1·14	4·18	gl, vp, hd, af, qtz, ox
8	1480	699	18	690	1·00	−1·12	*4·87*	gl, vp, hd, ox, (af)
9	1480	699	18	690	0·89	−1·22	*4·23*	gl, vp, hd, af, qtz, ox
22	1490	788	25	306	0·50	−1·80	2·49	gl, vp, hd, af, qtz, ox
31[5]	1558	693	24	1000	0·79	−1·55	—	vp, hd, af, qtz, znr, ox, richt
33	1558	693	24	1000	0·58	−1·82	*2·42*	gl, vp, af, qtz, bt, fay, ox
37	1505	661	30	951	1·00	−1·66	*4·87*	gl, vp, af, qtz, fay, bt, fl, ox
42[6]	1515	758	22	959	0·10	−3·13	*0·88*	gl, vp, qtz, af, fay, bt, fl, ox, richt
43[6]	1515	729	22	959	0·10	−3·20	*1·08*	gl, vp, qtz, af, fay, bt, fl, ox
44[6]	1515	773	22	959	0·10	−3·10	*0·96*	gl, vp, qtz, af, fay, fl, ox, richt
150 MPa, oxidized								
12	1550	794	0·04	407	1·00	4·39	4·84	gl, vp, ox
13	1550	794	0·04	407	0·90	4·30	4·14	gl, vp, ox
14	1550	794	0·04	407	0·80	4·20	3·75	gl, vp, ox
15	1550	794	0·04	407	0·68	4·06	3·52	gl, vp, hd, af, pl, ox
16	1550	794	0·04	407	0·59	3·93	2·08	gl, vp, hd, af, qtz, ox, fl
17	1520	752	0·04	502	1·00	4·29	4·66	gl, vp, ox, chevk
18	1520	752	0·04	502	0·89	4·19	4·22	gl, vp, hd, ox, (af), tit
19	1520	752	0·04	502	0·80	4·10	3·93	gl, vp, hd, af, ox, tit
20	1520	752	0·04	502	0·68	3·96	*3·00*	gl, vp, hd, af, qtz, ox, tit
21	1520	752	0·04	502	0·61	3·86	*2·59*	gl, vp, af, qtz, ox, fl
23	1550	696	0·04	1222	1·00	4·17	*4·87*	gl, vp, hd, af, ox, tit
24	1550	696	0·04	1222	0·90	4·08	*4·29*	gl, vp, hd, af, qtz, ox
25	1550	696	0·04	1222	0·79	3·97	*3·64*	gl, vp, hd, af, qtz, ox, fl
26	1550	696	0·04	1222	0·67	3·83	*2·94*	vp, hd, af, qtz, ox
27	1550	696	0·04	1222	0·59	3·72	*2·47*	vp, hd, af, qtz, ox
38[6]	1500	784	0·05	1138	0·10	2·35	*1·04*	gl, vp, af, qtz, ox, fl
50 MPa, reduced								
10	503	794	14	423	1·00	−1·48	3·72	gl, vp, hd, ox
11	503	794	14	423	0·80	−1·67	2·81	gl, vp, hd, af, ox
28	520	790	15	617	0·70	−1·82	2·19	gl, vp, hd, af, ox
29	520	790	15	617	0·61	−1·94	3·40	gl, vp, hd, af, qtz, ox, ap
30	520	790	15	617	0·50	−2·11	2·50	gl, vp, hd, af,qtz,ox
34	566	756	13	867	1·00	−1·36	2·58	gl, vp, hd, af, ox
35	566	756	13	867	0·81	−1·54	3·11	gl, vp, hd, af, ox, qtz
36	566	756	13	867	0·63	−1·76	—	vp, af, qtz, ox
40	524	688	20	1138	0·82	−2·08	—	vp, af, qtz, bt, rbk-arf, fl
41	524	688	20	1138	0·63	−2·31	—	vp, af, qtz, ox
Sample BL 575								
150 MPa, reduced								
1	1540	798	26	255	1·00	−1·19	*5·79*	gl, vp
2	1556	798	25	378	0·91	−1·23	5·38	gl, vp
3	1556	798	25	378	0·81	−1·33	4·16	gl, vp
4	1505	798	23	354	0·71	−1·41	2·52	gl, vp, ox
5	1505	798	23	354	0·59	−1·54	2·79	gl, vp, ox
6	1608	746	20	617	1·00	−1·03	4·75	gl, vp, ox
7	1608	746	20	617	0·90	−1·12	4·67	gl, vp, ox, (qtz)
8	1480	700	18	690	1·00	−1·12	*5·79*	gl, vp, ox
9	1480	700	18	690	0·91	−1·20	*5·07*	gl, vp, ox
22	1490	788	25	306	0·47	−1·86	2·45	gl, vp, ox, (qtz)
23	1490	791	25	306	0·37	−2·06	*0·77*	gl, vp, qtz, af, ox
24	1490	791	25	306	0·28	−2·30	*0·01*	gl, vp, qtz, af

	P (bar)	*T* (°C)	P_{H2} (bar)	Duration (h)	XH_2O_{in}[1]	log fO_2[2] (ΔNNO)	H_2O[3] (wt %)	Run products[4]
33	1558	676	24	1000	0·78	−1·61	*4·03*	gl, vp, qtz, af, rbk-arf, chevk
34	1558	676	24	1000	0·65	−1·77	*3·00*	gl, vp, qtz, af, rbk-arf, fl
35	1558	676	24	1000	0·51	−1·98	1·88	gl, vp, qtz, af, rbk-arf, fl
47	1505	661	30	951	1·00	−1·66	*5·79*	gl, vp, rbk-arf, bt, ox, fl, (qtz)
48	1505	702	30	951	0·63	−1·94	*2·83*	gl, vp, qtz, af, rbk-arf, fl
49	1505	702	30	951	0·45	−2·23	*1·41*	gl, vp, qtz, af, rbk-arf
50	1505	702	30	951	0·31	−2·56	*0·29*	gl, vp, qtz, af, rbk-arf
56[6]	1515	758	22	959	0·10	−3·13	*0·80*	gl, vp, qtz, af, fl
57[6]	1515	729	22	959	0·10	−3·20	*1·28*	gl, vp, qtz, af, rbk-arf, fl
58[6]	1515	773	22	959	0·10	−3·10	*0·67*	gl, vp, qtz, af
150 MPa, oxidized								
12	1550	805	0·11	407	1·00	3·61	5·59	gl, vp, ox
13	1550	805	0·11	407	0·87	3·49	4·94	gl, vp, ox
14	1550	805	0·11	407	0·79	3·40	4·36	gl, vp, ox
15	1550	805	0·11	407	0·68	3·27	3·00	gl, vp, ox, (qtz)
16	1550	805	0·11	407	0·57	3·12	2·36	gl, vp, ox, qtz
17	1520	757	0·11	502	1·00	3·50	5·98	gl, vp, ox
18	1520	757	0·11	502	0·90	3·41	5·60	gl, vp, ox
19	1520	757	0·11	502	0·78	3·28	4·14	gl, vp, ox
20	1520	757	0·11	502	0·67	3·15	3·18	gl, vp, ox, (af)
21	1520	757	0·11	502	0·59	3·04	2·69	gl, vp, qtz, af, ox, fl
25	1550	703	0·11	1222	1·00	3·39	*5·79*	gl, vp, ox
26	1550	703	0·11	1222	0·87	3·27	*4·75*	gl, vp, ox
27	1550	703	0·11	1222	0·78	3·17	*4·03*	gl, vp, qtz, af, ox
28	1550	703	0·11	1222	0·67	3·04	*3·16*	gl, vp, qtz, af, ox
29	1550	703	0·11	1222	0·59	2·93	*2·52*	gl, vp, qtz, af, ox, fl
36	1550	678	0·05	955	1·00	3·97	*5·79*	gl, vp, ox, chevk, fl
37	1550	678	0·05	955	0·91	3·89	*5·07*	gl, vp, ox, chevk, fl, qtz, af
38	1550	678	0·05	955	0·80	3·78	*4·19*	gl, vp, ox, qtz, af, aeg, fl
39	1550	678	0·05	955	0·62	3·56	*2·76*	gl, vp, ox, qtz, af, aeg, fl
40	1550	678	0·05	955	0·46	3·30	*1·48*	vp, ox, fl, qtz, af, aeg, znr
41	1520	700	0·11	955	0·51	2·78	*1·88*	gl, vp, qtz, af, aeg, fl
42	1400	786	0·04	955	0·51	3·71	1·85	gl, vp, qtz, af, ox, fl
43	1400	786	0·04	955	0·39	3·48	1·98	gl, vp, qtz, af, ox
51[6]	1500	784	0·05	1138	0·10	2·35	*0·88*	gl, vp, qtz, af, ox, fl
50 MPa, reduced								
10	563	798	14	423	1·00	−1·38	3·25	gl, vp, ox
11	563	798	14	423	0·81	−1·56	3·29	gl, vp, ox
30	520	798	15	617	0·69	−1·83	2·76	gl, vp, ox
31	520	798	15	617	0·62	−1·92	2·68	gl, vp, ox, (qtz)
32	520	797	15	617	0·49	−2·12	2·25	gl, vp, ox
44	566	737	13	867	1·00	−1·38	3·32	gl, vp, ox
45	566	737	13	867	0·79	−1·59	3·83	gl, vp, ox, qtz, af, fl
46	566	737	13	867	0·57	−1·87	2·56	gl, vp, ox, qtz, af
53	524	686	20	1138	1·00	−2·10	—	gl, vp, qtz, af, rbk-arf, ox, fl
54	524	686	20	1138	0·82	−2·27	—	gl, vp, qtz, af, rbk-arf, ox, fl
55	524	686	20	1138	0·82	−2·62	—	gl, vp, qtz, af, rbk-arf, ox
Sample SMN 49								
150 MPa, reduced								
1	1540	797	26	162	1·00	−1·19	*5·73*	gl, vp
2	1556	796	25	378	0·89	−1·25	3·94	gl, vp
3	1556	796	25	378	0·76	−1·39	3·39	gl, vp
4	1505	796	23	354	0·71	−1·41	2·85	gl, vp, qtz
5	1505	796	23	354	0·55	−1·55	2·24	gl, vp, qtz, af
6	1608	744	20	617	1·00	−1·03	5·29	gl, vp
7	1608	744	20	617	0·90	−1·13	3·52	gl, vp, qtz
8	1480	703	18	690	1·00	−1·11	*5·73*	gl, vp
9	1480	703	18	690	0·86	−1·20	*5·19*	gl, vp, qtz
22	1490	796	25	306	0·50	−1·79	*2·99*	gl, vp, qtz

Table 2: continued

	P (bar)	*T* (°C)	P_{H_2} (bar)	Duration (h)	XH_2O_{in}[1]	log fO_2[2] (ΔNNO)	H_2O[3] (wt %)	Run products[4]
23	1490	796	25	306	0·40	−1·98	*2·45*	gl, vp, qtz, af
32	1558	678	24	1000	0·79	−1·59	*4·58*	gl, vp, qtz, af, rbk-arf, chevk
33	1558	678	24	1000	0·69	−1·71	*4·04*	gl, vp, qtz, af, rbk-arf, fl, mondt
34	1558	678	24	1000	0·50	−1·99	*2·99*	gl, vp, qtz, af, rbk-arf, fl
44	1505	661	30	951	1·00	−1·66	—	gl, vp, bt, fl, chevk
45	1505	702	30	951	0·62	−1·96	3·65	gl, vp, qtz, af, ox
46	1505	702	30	951	0·50	−2·14	2·99	gl, vp, qtz, af, ox
47	1505	702	30	951	0·27	−2·68	1·73	gl, vp, qtz, af, rbk-arf, ox
58[6]	1515	758	22	959	0·10	−3·13	*1·12*	gl, vp, qtz, af, fl
59[6]	1515	729	22	959	0·10	−3·20	*1·42*	gl, vp, qtz, af, rbk-arf, fl
60[6]	1515	773	22	959	0·10	−3·10	*0·96*	gl, vp, qtz, af
150 MPa, oxidized								
12	1550	775	0·05	407	1·00	4·17	5·93	gl, vp
13	1550	775	0·05	407	0·89	4·07	3·56	gl, vp
14	1550	775	0·05	407	0·75	3·92	3·75	gl, vp
15	1550	775	0·05	407	0·67	3·82	3·52	gl, vp
16	1550	775	0·05	407	0·54	3·64	2·77	gl, vp, qtz, af, chevk
17	1520	725	0·05	502	1·00	4·05	5·68	gl, vp, ox
18	1520	725	0·05	502	0·88	3·94	4·91	gl, vp, ox, chevk
19	1520	725	0·05	502	0·79	3·85	4·11	gl, vp, qtz, ox
20	1520	725	0·05	502	0·68	3·72	4·22	gl, vp, qtz, fl, ox
21	1520	725	0·05	502	0·63	3·65	3·66	gl, vp, qtz, af, ox
24	1550	679	0·05	1222	1·00	3·94	*5·73*	gl, vp, ox, chevk
25	1550	679	0·05	1222	0·87	3·82	*5·02*	gl, vp, qtz, af, aeg, ox
26	1550	679	0·05	1222	0·78	3·72	*4·53*	gl, vp, qtz, af, aeg, ox
27	1550	679	0·05	1222	0·67	3·59	*3·93*	gl, vp, qtz, af, aeg, ox, fl
28	1550	679	0·05	1222	0·59	3·48	*3·49*	gl, vp, qtz, af, aeg, ox
35	1520	700	0·11	955	0·78	3·12	4·91	gl, vp, qtz, af, aeg
36	1520	700	0·11	955	0·66	2·97	3·99	gl, vp, qtz, af, aeg, fl
37	1520	700	0·11	955	0·55	2·87	*3·27*	gl, vp, qtz, af, aeg
38	1520	700	0·11	955	0·50	2·73	*2·99*	gl, vp, qtz, af, aeg
39	1400	786	0·05	955	0·39	3·29	2·78	gl, vp, qtz, af
40	1400	786	0·05	955	0·23	2·83	2·41	gl, vp, qtz, af, fl
48[6]	1500	784	0·05	1138	0·10	2·16	*1·45*	gl, vp, qtz, af, aeg, ox, fl
50	1500	731	0·05	598	1·00	4·09	5·68	gl, vp, ox
51[7]	1500	731	0·05	598	fa	—	4·98	gl, vp, ox
52[7]	1500	731	0·05	598	fa	—	4·36	gl, vp, ox, qtz, (af)
53[7]	1500	731	0·05	598	fa	—	3·28	gl, vp, ox, qtz, af, fl
54[6]	1500	731	0·05	598	0·01	0·09	*1·64*	gl, vp, qtz, af, rbk-arf, fl
50 MPa, reduced								
10	563	802	14	423	1·00	−1·37	2·49	gl, vp, (fl), (bt)
11	563	802	14	423	0·80	−1·57	2·52	gl, vp, (fl)
29	520	798	15	617	0·64	−1·89	2·77	gl, vp
30	520	797	15	617	0·56	−2·01	2·70	gl, vp
31	520	797	15	617	0·50	−2·11	3·06	gl, vp
41	566	732	13	867	1·00	−1·39	3·32	gl, vp
42	566	732	13	867	0·82	−1·56	3·42	gl, vp, qtz, af
43	566	732	13	867	0·57	−1·88	3·02	gl, vp, qtz, af, fl
55	524	679	20	1138	1·00	−1·92	—	gl, vp, qtz, af, fl
56	524	679	20	1138	0·83	−2·08	—	gl, vp, qtz, af, rbk-arf
57	524	679	20	1138	0·55	−2·44	—	gl, vp, qtz, af, rbk-arf

[1]$XH_2O_{in} = H_2O/(H_2O + CO_2)$ loaded in the capsule (in moles). For nominally anhydrous experiments, the final fluid phase composition is arbitrarily set at $XH_2O = 0{\cdot}1$ except for charge 54 of composition SMN 49.
[2]ΔNNO = log fO_2(experiment)—log fO_2 (NNO; Pownceby & O'Neill, 1994).
[3]Water contents of glasses determined using the by-difference method. Numbers in italic are calculated as explained in the text.
[4]Phase abbreviations as given by Kretz (1983): gl, glass; vp, fluid; af, alkali feldspar; qtz, quartz; hd: ferrohedenbergite; fay, fayalite; ox, oxides; fl, fluorite; chevk, chevkinite; tit, titanite; richt, ferrorichterite; rbk-arf, riebeckite-arfvedsonite solid solution; aeg, aegirine; montd, montdorite; ap, apatite. Parentheses are for relict phases.
[5]Leaked capsule.
[6]Nominally anhydrous charge.
[7]Fluid-absent charge.

Montdorite, a tetrasilicic mica (Robert & Maury, 1979), was identified in one charge from SMN 49 (Table 2). The only phase in the natural samples not identified in this study is aenigmatite.

Minerals display euhedral shapes with sizes of 5–30 μm, except for the Na-amphibole and aegirine, which crystallize as stubby prisms over 100 μm long, and for oxides whose size rarely exceeds 5 μm. Close to the liquidus, crystallization is marked by the appearance of a few large individuals (Fig. 1a), whereas at lower temperatures, nucleation is more efficient than growth, giving rise to a large number of smaller crystals (Fig. 1b). Although relict phases are very rare (<0·5% by volume of the crystal), they are clearly distinguished on the basis of their larger size (>100 μm), their rounded shape (alkali feldspar, quartz), dissolution textures at their borders (alkali feldspar), a reaction zone surrounding the crystal (hedenbergite) or the presence of a rim compositionally different from the core. In the last texture, the rim in all cases has the same composition as small euhedral crystals that grew during the experiment. Rounded relicts of tectosilicates are observed only in cases where the charge is outside, yet close to, the stability field of the corresponding phase. All charges, including those nominally anhydrous, display evidence of fluid saturation in the form of evenly dispersed bubbles with sizes varying between 10 and 100 μm, some containing cubic minerals. This population of equilibrium bubbles is clearly distinguishable from the micrometric to sub-micrometric bubbles present in charges that experienced slow quench rates (Fig. 1b). The reason for nominally anhydrous melts to be fluid saturated may be the presence of Cl and F, elements that promote early fluid saturation compared with the purely hydrous condition (e.g. Webster, 1992, 1997).

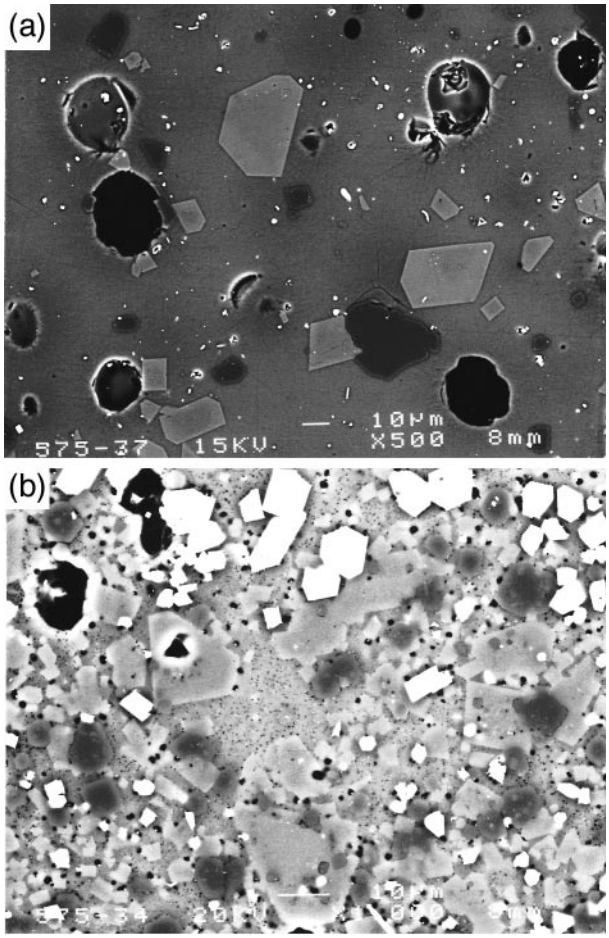

Fig. 1. Scanning electron micrographs of run products. In both pictures quartz has a dark grey to black shade compared with alkali feldspar. (a) Coexisting quartz and alkali feldspar crystals and glass in a near-liquidus charge of BL 575. Bright minerals are oxides. (b) Quartz, alkali feldspar and riebeckite–arfvedsonite (bright equant grains) and glass assemblage. (Note the presence of micron to sub-micron sized bubbles scattered throughout the charge, interpreted to occur during the quench.) The 10 μm large void in the upper left corner represents a former equilibrium fluid bubble.

Phase relationships

Phase relationships for the three compositions are shown in Figs 2–4. At 150 MPa, phase relations are shown in T–melt H_2O content projections. This type of projection could not be established at 50 MPa and only the T–XH_2O_{in} projection is shown. No attempt was made to establish the stability fields of zircon or apatite. The small size prevented in some cases clear identification of the type of Fe–Ti oxide. As a rule, magnetite grew in ND 002 whereas ilmenite or a Ti-bearing haematite crystallized in both BL 575 and SMN 49. Ilmenite is present, however, in some run products of ND 002, especially those whose fO_2 is significantly below NNO − 1. The nominally anhydrous runs performed under high and low fH_2 are also plotted. Despite the fact that their fO_2 may have been significantly below the fO_2 of H_2O–CO_2-bearing charges held under similar fH_2 conditions, both sets of charges display consistent phase assemblages, except for charge 54 in composition SMN 49 whose results conflict with the remainder. This point is discussed further below.

ND 002

At 150 MPa under reduced conditions (NNO − 1·6), magnetite and ferrohedenbergite are the liquidus phases, closely followed by alkali feldspar, quartz and then fayalite (Fig. 2a). At H_2O saturation, the crystallization temperatures of oxide and ferrohedenbergite are estimated to be close to 760°C, whereas alkali feldspar precipitates near 700°C, followed by quartz near 660°C. At melt H_2O content lower than 2–3 wt % and at temperatures higher than 700°C, hedenbergite is no longer stable and the main stable ferromagnesian silicate is fayalite,

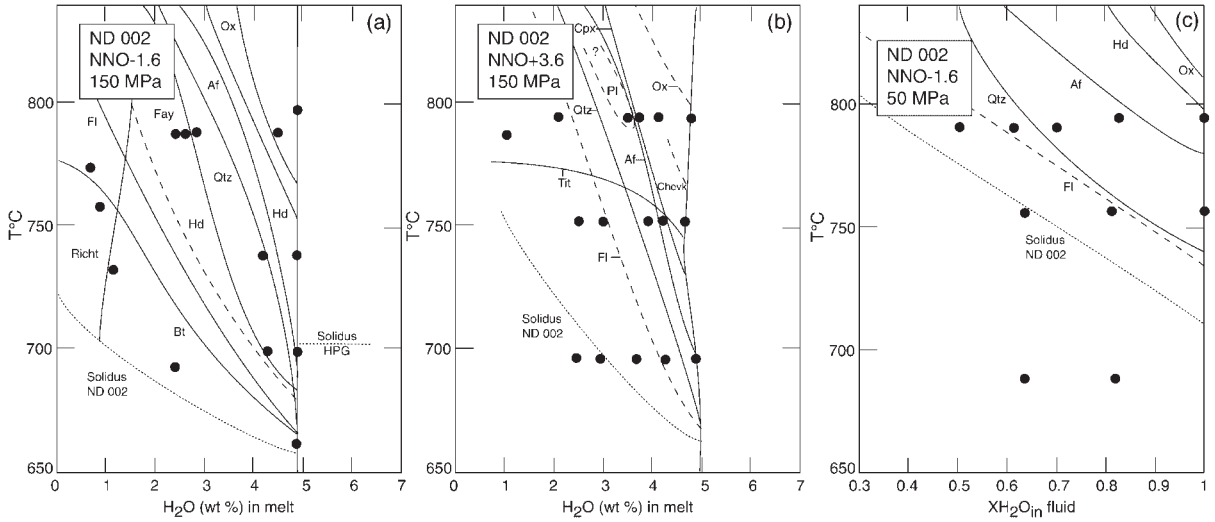

Fig. 2. Phase relationships of ND 002. Mineral abbreviations are as recommended by Kretz (1983). The curves are labelled with minerals lying inside their respective stability fields, and are shown dashed when inferred. (a) 150 MPa and NNO − 1·6; (b) 150 MPa and NNO + 3·6; (c) 50 MPa and NNO − 1·6. Solidus HPG is the solidus of the subaluminous haplogranite system at 150 MPa (Johannes & Holtz, 1996).

coexisting with ilmenite. At low H_2O_{melt} (<2 wt %) and temperatures above 730°C, a ferro-richteritic amphibole is present. Below 700°C amphibole is present only in a subsolidus charge (charge 31, Table 2), and the amphibole-out curve has a rather steep slope. In the dry charge at 729°C (charge 44, Table 2), a former hedenbergite phenocryst was found rimmed by fayalite, ilmenite and fluorite, suggesting that these phases replace pyroxene at low H_2O_{melt}. Finally, the scarce occurrence or absence of hedenbergite in charges at temperatures below 700°C suggests that its stability field may not extend down to the solidus in ND 002 in the water-rich part of the diagram. Thus, we have drawn a hedenbergite-out curve that is crossed either as temperature falls or as melt H_2O decreases. Biotite was identified only below 700°C at H_2O saturation, or in dry charges at higher temperatures, which suggests a restricted stability for fO_2 at or below NNO − 1·6, close to the solidus. Similarly, fluorite is present only in strongly crystallized charges or below 700°C at H_2O saturation and its stability field lies close to the solidus. Although not looked for systematically, chevkinite was not found. No attempt was made to locate the solidus precisely, but it is below 660°C at H_2O saturation (Table 2), which is 40°C lower than the solidus of the haplogranite system at 150 MPa (Johannes & Holtz, 1996). Melt H_2O contents at saturation are slightly lower than 5 wt %, being similar to those found in the metaluminous haplogranite system (Johannes & Holtz, 1996) at similar P and T.

Increased fO_2 does not alter the order of crystallization of the major phases (Fig. 2b) but it yields, at H_2O saturation, magnetite crystallization above 800°C, whereas clinopyroxene saturation occurs slightly below 750°C. Although the liquidus of the alkali feldspar at H_2O saturation may be higher by ~10°C, over most of the investigated domain and within the error in the melt H_2O determination, the crystallization temperatures of the tectosilicates remain unchanged relative to that at low fO_2. Biotite, fayalite and amphibole were not identified. In contrast, titanite is present in most of the 750°C charges and possibly in all the 700°C charges, and the titanite-in curve is drawn flat at temperatures close to 750°C. As at low fO_2, fluorite is present in some crystal-rich charges close to the solidus. Although data are lacking, its stability domain extends to higher temperatures, as seen under low fO_2. Chevkinite was identified in only one charge at H_2O saturation and 752°C, and its stability field is shown dashed with a shape similar to that seen in BL 575 and SMN 49 at high fO_2. The solidus seems to be at significantly higher temperature, by ~30°C, than under reduced conditions. This is apparent when comparison is made between charge 33, which contains at least 10% residual glass by volume as estimated from scanning electron micrographs, and charge 27, which has no clear textural evidence of residual glass, despite the fact that both charges have similar XH_2O_{in} values and were run at almost identical temperatures. Finally, plagioclase was identified (by EMPA) in charge 15 run at ~790°C under relatively dry conditions. This is the only instance of plagioclase crystallization in this study. Charges bracketing charge 15 do not contain plagioclase and it does not appear at lower temperature, implying a closing of the plagioclase stability field, if any, at low temperature.

Decreasing the pressure to 50 MPa under low fO_2 does not affect the relative order of crystallization, although

fayalite has not been identified (Fig. 2c). The liquidus temperatures of all phases at H_2O saturation are significantly raised, by ~60°C, for the tectosilicates. Alkali feldspar-in and quartz-in curves are more clearly separated from each other, suggesting that these two phases are not equally sensitive to changes in pressure. Biotite and Na-amphibole have been identified only in some subsolidus charges at ~690°C (Table 2), but their stability in the presence of liquid cannot be ruled out. The solidus at H_2O saturation is probably close to 700°C, that is, 60°C lower than that of the haplogranite system at 50 MPa. Melt H_2O contents at saturation range from 2·6 to 3·7 wt %, although the lower figure is probably correct (Table 2).

BL 575

This composition is a typical comendite with higher FeO_{total} and Na_2O contents than ND 002. At 150 MPa under reduced conditions, an oxide is the liquidus phase, crystallizing at 750°C and H_2O saturation (Fig. 3a). It is followed by alkali feldspar and quartz, crystallizing simultaneously over the T–H_2O_{melt} range explored. Their temperature of appearance at H_2O saturation is slightly higher than 650°C. Fluorite was found mainly in low-temperature charges, where it usually crystallizes at lower temperature than amphibole, except at H_2O saturation. Under dry conditions, the maximum thermal stability of fluorite does not exceed 775°C. At H_2O_{melt} >3 wt %, Na-amphibole crystallization is restricted to temperatures below 700°C. Its crystallization at H_2O saturation occurs slightly above 660°C. Under nominally dry conditions its thermal stability extends to near 740°C. Biotite is present only at the lowest temperature investigated and at H_2O saturation, where it is a near-liquidus phase together with amphibole and fluorite. Its liquidus curve displays a positive slope in the T–H_2O_{melt} projection, but the exact shape of this boundary is not yet well constrained. The chevkinite stability field seems to be restricted to low melt H_2O contents (Table 2), but is also poorly constrained. Melt H_2O contents at saturation are slightly lower than 6 wt %, being 1 wt % higher than those of ND 002. The solidus has not been located but is definitely below 650°C at H_2O saturation, possibly close to, or even below, 600°C.

Increasing fO_2 by 5 log units increases the thermal stability of Fe–Ti oxide (Fig. 3b). Below 750°C, quartz and alkali feldspar appear to be insensitive to variations in fO_2. Fluorite crystallizes at ~680°C at water saturation, and its liquidus roughly parallels that of the tectosilicates over the temperature range investigated. In contrast to low fO_2, its thermal stability seems largely to exceed 800°C. Chevkinite may have a slightly wider stability field relative to low-fO_2 conditions. Under H_2O saturation it is the second phase to precipitate after oxide at ~690°C. Its thermal stability when H_2O_{melt} decreases is again not well constrained. Both Na-amphibole and biotite are absent at high fO_2. The former is replaced by aegirine whose thermal stability also increases as H_2O_{melt} decreases. Solidus conditions were approached at 678°C in charge 40 (XH_2O_{in} = 0·46); no glass is seen on SEM images. Comparison with results at low fO_2 (charge 35 at 676°C and XH_2O_{in} 0·51 has >20% glass in volume) again suggests that a rise in fO_2 produces a rise in solidus temperatures, as in ND 002. Melt H_2O contents required for quartz and alkali feldspar saturation at any given temperature are identical to those at low fO_2.

Decreasing the pressure to 50 MPa raises the crystallization temperatures by ~50–60°C (Fig. 3c), as for ND 002. Quartz appears before alkali feldspar but the less extensive coverage of T–H_2O_{melt} data prevents accurate location of the phase boundaries. Melt H_2O contents at saturation are in the range 3·2–3·5 wt % (Table 2). At H_2O saturation, the Na-amphibole stability field is higher by ~30°C compared with that at 150 MPa. Biotite was not identified; if stable, it must crystallize below 680°C, as tentatively suggested in Fig. 3c.

SMN 49

This composition is close to BL 575, differing only in a slightly higher SiO_2 content (Table 1). The phase relations of SMN 49 are thus essentially the same as those of BL 575 (Fig. 4), except that at low fO_2 no stability field for Fe–Ti oxides could be established. The liquidus curves of quartz and alkali feldspar are also more clearly separated from each other. Montdorite was recognized (by EMPA) in only one low-fO_2 and near-solidus charge (33, Table 2).

At high fO_2 under H_2O-saturated conditions, Fe–Ti oxide crystallizes at slightly over 730°C, followed by chevkinite at ~720°C. The thermal stability of chevkinite is significantly larger than that in BL 575. The dry charge at 731°C (54) yielded Na-amphibole and no pyroxene (Table 2). This difference is interpreted as due to a significantly lower fO_2 relative to the H_2O–CO_2-bearing charges, possibly resulting from less adsorbed water in the powder loaded to charge 54. This charge has been ignored in establishing the phase relations at high fO_2. As for BL 575, a rise in fO_2 produces a marked rise in the solidus temperature, best seen when comparing charges 38 and 46, which have the same T–H_2O_{melt} location but were run under different fO_2 conditions (Table 2). Whereas charge 38 (high fO_2) shows a minimal amount of residual glass in scanning electron micrographs, charge 46 (low fO_2) displays a much larger fraction of residual glass. A further feature of interest is that the crystallization sequence produced at ~730°C with the H_2O-undersaturated but CO_2-free charges

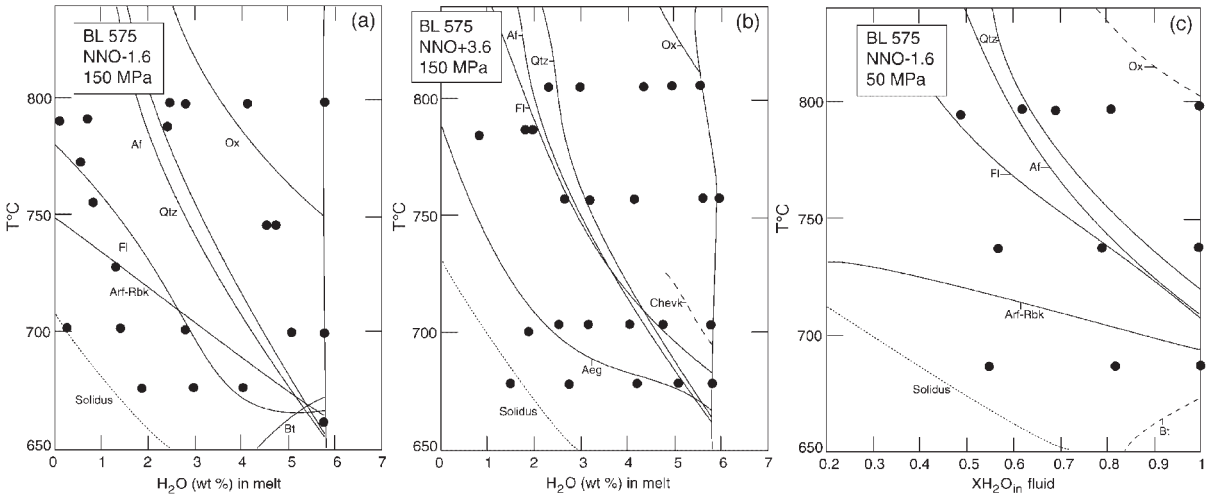

Fig. 3. Phase relationships of BL 575. Mineral abbreviations are as recommended by Kretz (1983). The curves are labelled with minerals lying inside their respective stability fields, and are shown dashed when inferred. (a) 150 MPa and NNO − 1·6; (b) 150 MPa and NNO + 3·6; (c) 50 MPa and NNO − 1·6.

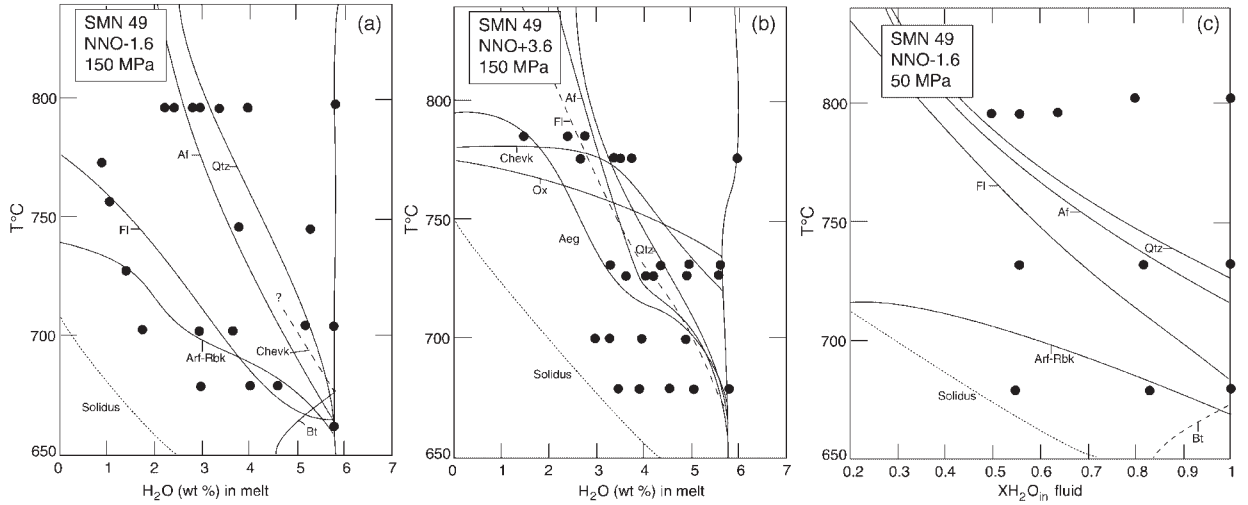

Fig. 4. Phase relationships of SMN 49. Mineral abbreviations are as recommended by Kretz (1983). The curves are labelled with minerals lying inside their respective stability fields, and are shown dashed when inferred. (a) 150 MPa and NNO − 1·6; (b) 150 MPa and NNO + 3·6; (c) 50 MPa and NNO − 1·6.

(charges 50–53) is virtually identical, both in terms of phase assemblages and T–melt H_2O coordinates, to that obtained in CO_2-bearing charges (charges 17–21), or within the analytical error of our melt H_2O content determination technique.

At 50 MPa, at H_2O saturation, the crystallization of both quartz and alkali feldspar occurs around 725°C (Fig. 4c), or 60°C higher than at 150 MPa. The fluorite-in curve possibly has the same relative position as at 150 MPa. Melt H_2O contents at saturation are identical to those determined for BL 575 (Table 2). Amphibole stability is slightly expanded towards higher temperature. Biotite is not present under the experimental conditions investigated at 50 MPa. If this mineral crystallizes in SMN 49 it must do so below 680°C.

DISCUSSION

Aenigmatite stability

Our phase equilibrium experiments successfully reproduced the phase assemblages of the rocks, apart from aenigmatite. Several factors may have contributed to this. The low modal abundance of aenigmatite in the rock

suggests that this phase may also have crystallized in such low amounts in the experiments that it was overlooked in the run products. However, phases present in equally low amounts were identified, e.g. biotite and fayalite. Previous experimental studies do not mention difficulties in growing aenigmatite under laboratory conditions similar to ours (Ernst, 1962; Thompson & Chisholm, 1969; Lindsley 1971). Rather, an inappropriate choice of one or more of the intensive parameters may have prevented aenigmatite crystallization. The experimental work of Ernst (1962) on a synthetic Na–Fe end-member amphibole has shown that Ti-free aenigmatite is unstable at pressures >90 MPa. Thompson & Chisholm (1969) synthesized Ti-bearing stoichiometric aenigmatite at 100 MPa, which suggests that Ti enhances the pressure stability of this phase. Although there are currently no data on aenigmatite stability at pressures >100 MPa, its stability may be pressure dependent, possibly explaining its absence in our experiments. On the other hand, Ernst (1962) and Lindsley (1971) showed that the occurrence of aenigmatite also depends on redox conditions, being enhanced at low fO_2. Ti-free aenigmatite is unstable at fO_2 above that of the wüstite–magnetite solid buffer whereas the Ti-bearing variety is stable to an fO_2 between NNO and FMQ. Although our lowest fO_2 is in the correct range for stoichiometric Ti-bearing aenigmatite to crystallize, a small departure of the natural aenigmatite composition from the theoretical one of Lindsley (1971) may affect the fO_2 stability of that phase in the rock. It is therefore possible that our imposed fO_2 may not have been sufficiently low to stabilize aenigmatite, even at the lowest pressure investigated here.

Comparison between ND 002, BL 575 and SMN 49

At 150 MPa, liquidus temperatures are higher in ND 002, consistent with the fact that it represents the least differentiated member of the GOVC rhyolite suite. However, comparing only the tectosilicates, which are >90% of the crystallizing assemblage, the liquidus temperature of ND 002 is only 30°C higher than those of BL 575 and SMN 49. The phase relations established at 50 MPa suggest that the positions of tectosilicate liquidi are more sensitive to composition at decreasing pressures, this being most apparent for the liquidus temperature of alkali feldspar in ND 002, which is significantly higher than in the two more peralkaline compositions. As regards crystallization sequence, the liquidus tectosilicate in ND 002 is alkali feldspar, cotectic quartz–alkali feldspar crystallization is observed in BL 575, and quartz crystallizes before alkali feldspar in SMN 49. Although this may partly be due to anhydrous compositional variations, the influence of other volatiles is possible. The fact that CO_2-free and CO_2-bearing charges yield essentially the same results in SMN 49 shows that this volatile has a limited solubility in peralkaline silicic melts and that it mainly acts as a diluting agent in the fluid phase, as documented for other silicic magmas at low pressures (e.g. Blank *et al.*, 1993). Differences in CO_2 solubility cannot therefore explain the observed differences in liquidus minerals. In contrast, fluorine expands the primary volume of quartz in the haplogranite system (Manning, 1981). The combined effects of the slightly more silicic composition of SMN 49 compared with BL 575 and the fluorine complexing effect in alumino-silicate melts may explain why the quartz-in curve is more clearly separated from that of alkali feldspar in SMN 49 than in BL 575.

Montdorite has been identified in SMN 49 only but may be present in BL 575 as well. The stability domain of this phase needs refinement but our data agree with published occurrences of montdorite in magmatic rocks (e.g. Robert & Maury, 1979). Montdorite was first described in a comendite sill (Robert & Maury, 1979), where it occurs in the groundmass along with manganoan arfvedsonite, quartz, anorthoclase, oxides and fluorite among other accessory phases. T–fO_2 conditions of crystallization obtained from two-oxide geothermometry were 760°C and NNO, pointing to low temperature and moderately reduced fO_2 during montdorite crystallization. This estimate, together with the textural evidence and our experimental data, all suggest that montdorite occurs only late in the crystallization sequence of comendite magmas. On the basis of the relationships in SMN 49, we suggest that montdorite may replace biotite as the stable ferromagnesian potassic phase, when the residual liquid becomes strongly peralkaline.

It is well known that substitution of fluorine for hydroxyl groups in hydrous minerals such as amphibole can substantially raise their thermal stability, as shown, for instance, by Holloway & Ford (1975) for pargasite. The Na-amphibole produced in our work has a F content of $\sim$2 wt % at H_2O saturation. Despite this, the thermal stability of this phase in comendite magma at H_2O saturation does not exceed 670°C, which is lower than the upper stability limit of pure OH-riebeckite in H_2O fluid (Ernst, 1962).

The fluxing effect of the volatiles is well illustrated using the phase relationships obtained on ND 002, which most closely approached solidus conditions in this study. In Fig. 2, the solidus of the haplogranite system at 150 MPa at H_2O saturation (Johannes & Holtz, 1996) is shown in the ND 002 phase diagram obtained at 150 MPa. The difference between the two solidi is at least 40°C. The reason for such a low solidus temperature in ND 002 is the presence of additional components relative to the metaluminous base composition of the haplogranite system, most notably Fe, F and Cl. Previous experimental studies have shown that these components depress solidus temperatures to some extent in granitic

systems (Wyllie & Tuttle, 1961; Abbott, 1981; Manning, 1981; Pichavant *et al.*, 1987; Webster *et al.*, 1987; Weidner & Martin, 1987).

Comparison with previous work

Only a few experimental studies have been performed on natural peralkaline silicic rocks, notably by Bailey and co-workers, who determined the liquidus relations, under both hydrous and anhydrous conditions, of several pantelleritic obsidians (Bailey & Cooper, 1978). The redox conditions of their H_2O-saturated experiments were imposed by the vessel, and were presumably relatively oxidizing, above NNO + 1. The more peralkaline nature of their starting product, in combination with our three starting materials, allows us to establish the effect of peralkalinity on the near-liquidus phase relations of peralkaline magmas at H_2O saturation and high fO_2. In pantellerites at 150 MPa, quartz crystallizes at 650°C, whereas alkali feldspar is the liquidus tectosilicate appearing at ~690°C. Comparison with BL 575 and SMN 49 at high fO_2 (Figs 3b and 4b) shows that the alkali feldspar stability field is slightly expanded in pantellerites relative to comendites, whereas quartz preserves its position. In ND 002, the least peralkaline composition, quartz and alkali feldspar have liquidus temperatures equal to, or only marginally higher than, those in the other comendites and pantellerites. In pantellerites, the liquidus phase at high fO_2 is an acmitic pyroxene. It crystallizes at 760°C or ~100°C higher than in comendites at H_2O saturation (Figs 3 and 4).

Bailey & Cooper (1978) did not perform H_2O-saturated and low-fO_2 experiments, which prevents direct comparison with our results obtained at low fO_2. Their low-fO_2 experiments (thought to be around FMQ) were nominally anhydrous. However, a qualitative agreement in the phase assemblage is observed between the two datasets. In pantellerites, aegirine is absent (but a sodic hedenbergite is reported) whereas a sodic amphibole crystallizes at ~750°C, i.e. 10–20°C higher than in the comendites under the driest conditions investigated in our study. Thus, it appears that the increase of agpaicity in peralkaline silicic magmas does not produce any appreciable effect on tectosilicate liquidus temperatures. In contrast, mineral phases typifying the peralkaline condition, such as aegirine and Na-amphibole, have their stability fields expanded when peralkalinity increases, by ~100°C from comendites to pantellerites in the case of aegirine.

Temperatures of the liquidus minima in synthetic peralkaline acid systems at 100 MPa (Carmichael & Mackenzie, 1963; Thompson & Mackenzie, 1967), both iron free and iron bearing, are in the range 715–690°C (Carmichael & Mackenzie, 1963), slightly higher than those obtained in the present study. At 100 MPa and H_2O saturation, composition ND 002 falls on the quartz–alkali feldspar cotectic at 700°C, whereas BL 575 and SMN 49 do so at 680°C (the values at 100 MPa for our three compositions have been obtained by linear interpolation of the data obtained at 50 and 150 MPa). Minimum cotectic temperatures in the haplogranite system are higher by 20–30°C, i.e. 720°C at 100 MPa (Tuttle & Bowen, 1958). The tight grouping of quartz–feldspar cotectic temperatures (in the range 680–720°C) in synthetic and natural systems encompassing a large range of agpaitic indices shows that peralkalinity does not induce a marked depression in liquidus temperatures of tectosilicates in H_2O-saturated silicic magmas, which contrasts with the situation under dry conditions (Bailey & Schairer, 1966). The fact that the cotectic temperatures are slighty lower in this work than in the related synthetic systems may rather be attributed to the role of other volatiles (F, Cl). The addition of 1 wt % F to the H_2O-saturated haplogranite system at 100 MPa produces a fall in the temperature of the minimum of 35°C (Pichavant & Manning, 1984). Such an effect is similar in magnitude to that observed in the present study for the two comendites with ~1 wt % F, whose cotectic temperature is lower by ~20°C than their synthetic F-free counterparts.

Plagioclase stability in silicic magmas

Phase relationships have been established for both metaluminous (Webster *et al.*, 1987) and peraluminous (Bénard *et al.*, 1985; Pichavant *et al.*, 1987; London *et al.*, 1989) silicic rock compositions. Considering first the metaluminous rocks, Webster *et al.* (1987) worked on an F-enriched vitrophyre (1·2 wt % F). Apart from its higher Al_2O_3 and lower FeO_{tot} contents, the vitrophyre composition is similar to that of ND 002. At 100 MPa under H_2O saturation, both compositions crystallize the tectosilicates at 700°C. However, in the vitrophyre, two feldspars crystallize, unlike the case in ND 002 (Fig. 2). This is despite the fact that both rock compositions have almost identical bulk CaO content (0·40 wt % for the vitrophyre), and the vitrophyre is slightly more potassic than ND 002 (5·1 and 4·7 wt %, respectively). This suggests that even a slight deficit in Al_2O_3, such as in ND 002, inhibits plagioclase crystallization at the expense of alkali feldspar and quartz in silicic magmas. This is in accord with general petrographic evidence; in a compilation of 104 analyses of comendites and pantellerites, only one rock (from Oraefajokull, Iceland) clearly contained plagioclase phenocrysts (Macdonald & Bailey, 1973). At all water contents quartz is the liquidus phase in the vitrophyre, closely followed by sanidine and then plagioclase, the reverse of that in ND 002 (Fig. 2). This relative crystallization order is opposite to that predicted

from the normative quartz content of the bulk rocks (higher in ND 002 than in the vitrophyre). As proposed by Webster *et al.* (1987), such a crystallization sequence in the vitrophyre probably results from fluorine expanding significantly the primary volume of quartz relative to coexisting feldspars in the haplogranite system (Manning, 1981). With respect to the minor phases, the vitrophyre lacks clinopyroxene and oxides but biotite displays a larger stability field than in ND 002. Both topaz and fluorite crystallize in the vitrophyre, yet neither phase approaches liquidus conditions (<50–75°C below), unlike fluorite in the two comendites studied here. Overall, it appears that plagioclase crystallization in Ca-poor silicic melts is not suppressed by the addition of these levels of fluorine, as it has crystallized in the F-rich vitrophyre and not in the F-poorer ND 002 sample.

For F-poor peraluminous silicic magmas, comparison of our results with those obtained by Bénard *et al.* (1985) shows that, in peraluminous melts, quartz and alkali feldspar crystallize at similar temperatures (710°C at H_2O saturation and 100 MPa) to ND 002, our F-poor, least peralkaline composition. Unlike in ND 002, however, plagioclase precipitates at ~770°C at 100 MPa in the peraluminous system despite bulk calcium contents on average similar to, or even lower than, those of the rocks used in our study [between 0·38 and 0·54 wt % for the three natural compositions used by Bénard *et al.* (1985)]. Experimental work on various F, Li, B-enriched peraluminous granites (Pichavant *et al.*, 1987; London *et al.*, 1989) showed also that all three major tectosilicates are stable in these magmas. Again, despite bulk CaO contents of ~0·2 wt %, plagioclase is the liquidus tectosilicate, closely followed by quartz and alkali feldspar. All peraluminous silicic rocks lack fluorite, despite bulk F contents in the range 1·2–2·4 wt %. The above observations suggest therefore that lack of plagioclase crystallization in peralkaline magmas is directly linked to the intrinsic peralkaline character of the melt and not to an unusual deficit in CaO.

Role of fO_2 on the phase relations of peralkaline magmas

The phase relations displayed in Figs 2–4 help in understanding the main effects of fO_2 variations in peralkaline silicic magmas. For the three rock compositions, variations in fO_2 do not significantly affect the liquidus curves of quartz and alkali feldspar. The main exception is plagioclase crystallization in ND 002, which apparently occurs under oxidizing conditions only. The alkali feldspar liquidus in ND 002 may also be slightly enhanced under high fO_2. Overall, this indicates that feldspar- and quartz-producing species in the melt are not affected by fO_2. As variations in fO_2 primarily affect the Fe^{2+}/Fe^{3+} ratio of silicate melts, this in turn suggests that quartz and alkali feldspar melt components are not directly linked to iron in the melt structure. This contrasts with the experimental observations of Dall'Agnol *et al.* (1999) on a metaluminous silicic composition. By establishing the phase relationships under two widely different sets of redox conditions (NNO − 1 and NNO + 2·5), they showed that a rise in fO_2 produces a significant increase in the thermal stability of the tectosilicates, the effect being most dramatic for the feldspars, especially plagioclase. This strong dependence of plagioclase stability on fO_2 suggests an intimate association between the feldspar melt components and the iron species in iron-bearing metaluminous silicic melts. Such a relationship appears not to exist in relatively F-rich peralkaline silicic melts.

In contrast to the tectosilicates, all other phases crystallizing in the peralkaline rocks are sensitive to fO_2 to various degrees. In all three compositions, an increase in fO_2 is marked by an increase in the thermal stability of oxides, an effect similar to that seen in almost all Fe-bearing magmas. The accessory phase chevkinite also displays an expansion of its stability field as fO_2 increases (Fig. 4), especially in SMN 49, where its stability rises by ~50°C when fO_2 increases. Differences in the stability fields of chevkinite in BL 575 and SMN 49 are possibly related to different trace element contents of the bulk rocks but could be due also to difficulties in distinguishing chevkinite from oxide in BL 575, unlike in SMN 49. Fayalite in ND 002 and biotite in all three rocks apparently are stable only at low fO_2. The Ca-rich pyroxene is present in ND 002 whatever fO_2 prevails but its thermal stability is lowered when fO_2 increases. Titanite is present under oxidizing conditions only, as in metaluminous silicic magmas (e.g. Wones, 1989; Dall'Agnol *et al.*, 1999) and its crystallization may in part explain the diminished stability field for the Ca-pyroxene at high fO_2, as both phases compete for Ca in liquid. One of the most significant changes produced by the increase in fO_2 is the replacement in the low-temperature range of Na-amphibole by aegirine. The fact that both phases display similar stability fields suggests that they are related to each other through a redox reaction (Deer *et al.*, 1978). Given that the amphibole is strongly enriched in F, and that aegirine accommodates no F in its structure, amphibole breakdown must release F. This F release may in part explain the slighty enhanced stability field of fluorite under oxidizing conditions.

The last important feature with respect to fO_2 concerns its influence upon the solidus. Although non-systematic, the data reported here clearly show that peralkaline silicic magmas at low fO_2 can have solidus temperatures significantly lower than at high fO_2. We estimate that the lowering of solidus temperatures as a result of decreasing fO_2 from NNO + 3·6 to NNO − 1·6 is at

least 30°C and could be as high as 50°C, the magnitude of the effect increasing with the bulk iron content. Clearly, this relies on the solution properties of iron in silicate melts and their dependence on fO_2. One implication is that crystal fractionation in peralkaline silicic magmas will be enhanced by low fO_2. Another is that a peralkaline protolith will start melting at a lower temperature under low fO_2 rather than high fO_2. This redox melting mechanism has been already proposed by Bailey (1974) for mafic systems.

Role of pressure

Variation in pressure between 50 and 150 MPa in our study does not produce any fundamental change in the phase relationships, apart perhaps for aenigmatite stability. In particular, the relative order of crystallization of alkali feldspar and quartz remains unaltered. Anhydrous pantellerites, on the other hand, exhibit a change in their liquidus phase with pressure, quartz replacing alkali feldspar at pressures >100 MPa (Bailey *et al.*, 1974). In pantellerites, the stability of Na-amphibole extends down to near-atmospheric pressure (Bailey & Cooper, 1978) and is weakly sensitive to pressure. Such behaviour is here confirmed for the riebeckite–arfvedsonite variety, showing furthermore that, in comendite magma, not only is amphibole stable at low pressure but its thermal stability increases with decreasing pressure, albeit slightly in the pressure range investigated. The thermal stability of amphibole at H_2O saturation at 50 MPa, where the melt H_2O content is 3·3 wt % H_2O, is similar to that at 150 MPa for a melt H_2O content of 3 wt %. Thus, it can be expected that at P <50 MPa, the thermal stability of amphibole may still increase to reach the maximum observed under anhydrous conditions at 150 MPa, 730–740°C. In the least peralkaline composition, amphibole replaces clinopyroxene at low water activity, the opposite behaviour to the amphibole–pyroxene relationship observed in all metaluminous melts so far worked on (e.g. Martel *et al.*, 1999; Scaillet & Evans, 1999). Amphibole stability in peralkaline magmas is thus fundamentally different from that in calc-alkaline, silicic to intermediate magmas, where amphibole crystallization demands melt water contents >4 wt % (e.g. Scaillet & Evans, 1999), and where it is hardly stable at pressures below 50–100 MPa (e.g. Sato *et al.*, 1999). The contrast is probably partly related to the fact that amphiboles in peralkaline magmas are more F rich. Thus, the crystallization of amphibole in peralkaline silicic magmas does not appear to be a reliable indicator of water pressure. Rather, its occurrence in mildly peralkaline rhyolites mainly indicates that both low-fO_2 and low-temperature conditions prevailed in the magma chamber. Biotite does not follow the same pattern, as this phase is not stable at low pressure, at least under near-liquidus conditions. Biotite crystallization in comendite magmas at near-liquidus conditions implies pressures of at least 150 MPa.

Our experimental data help constrain the mineralogical evolution, mostly the behaviour of quartz, alkali feldspar and amphibole, of an ascending peralkaline magma under various T–H_2O_{in} melt conditions. For this purpose, the stability curves of some critical phases in a P–T projection are shown in Figs 5 and 6. In ND 002 at H_2O saturation (Fig. 5), the appearance curves of all major crystallizing phases (quartz, feldspar, clinopyroxene and magnetite) display negative slopes, which implies that, if ascent takes place at constant temperature under equilibrium conditions, extensive crystallization of the magma should occur. In contrast, if the magma starting conditions are below H_2O saturation, the appearance curves display a positive slope, down to the pressure at which the magma reaches H_2O saturation (Fig. 5). As illustrated for quartz in ND 002, the slope of the liquidus increases progressively as the bulk H_2O content of the magma decreases. A magma starting at 150 MPa, 740°C, with 4 wt % H_2O, will soon dissolve quartz upon rising, but it will do so only until 100 MPa, where it reaches H_2O saturation. Beyond, quartz crystallization will take place again. In contrast, a magma ascending from 150 MPa, 790°C and 2·5 wt % H_2O will intersect the quartz saturation boundary only at very low pressures, around 10 MPa. The alkali feldspar liquidus is reached at slightly higher pressures, at around 25 MPa. A similar line of reasoning shows that compositions BL 575 and SMN 49, both starting at 150 MPa, 760°C and 3 wt % H_2O, will reach the cotectic condition at $\sim$25 MPa (Fig. 6). The relatively weak dependence of amphibole thermal stability on pressure implies that this phase will persist upon rising, unlike in calc-alkaline magmas. Instead, amphibole crystallization may take place at very shallow levels where dehydration of the magma occurs, thus raising amphibole thermal stability. This probably explains the common occurrence of amphibole microlites in the groundmass of volcanic rocks. For instance, an H_2O-saturated magma residing at 150 MPa and 700°C, i.e. outside the amphibole stability field, will upon ascent and concomitant degassing cross the amphibole liquidus at 40 MPa and end its ascent with abundant microlites, but no phenocrysts, of amphibole (Fig. 6).

This general picture is similar overall to that for other types of silicic magmas (Johannes & Holtz, 1996). It indicates that, to preserve their near-liquidus character up to near-surface conditions, peralkaline magmas must be H_2O undersaturated, unless ascent rates are fast enough to prevent chemical reaction. The fact that many peralkaline rocks display dissolution textures, such as rounded or embayed quartz phenocrysts (Sutherland, 1974; Barclay *et al.*, 1996), may potentially be related

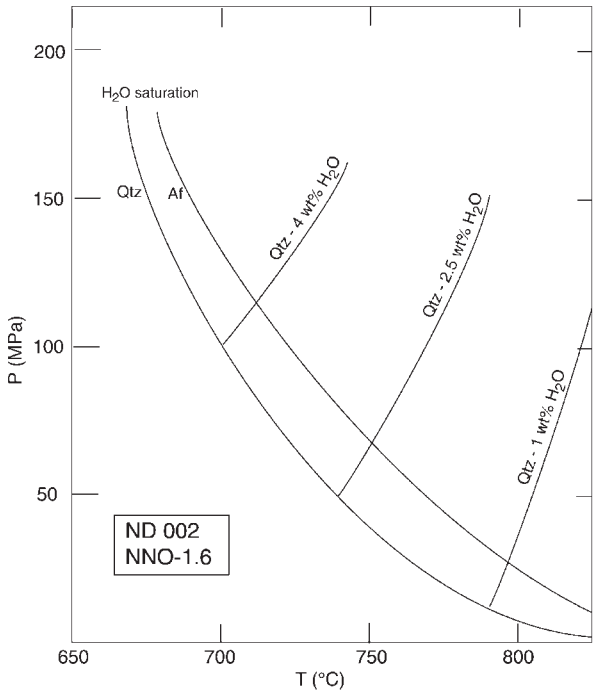

Fig. 5. *P–T* stability curves for quartz and alkali feldspar in ND 002 at H_2O saturation. The stability curves of quartz for a magma containing 1, 2·5 and 4 wt % H_2O are also shown. The curves are labelled with minerals lying inside their respective stability fields.

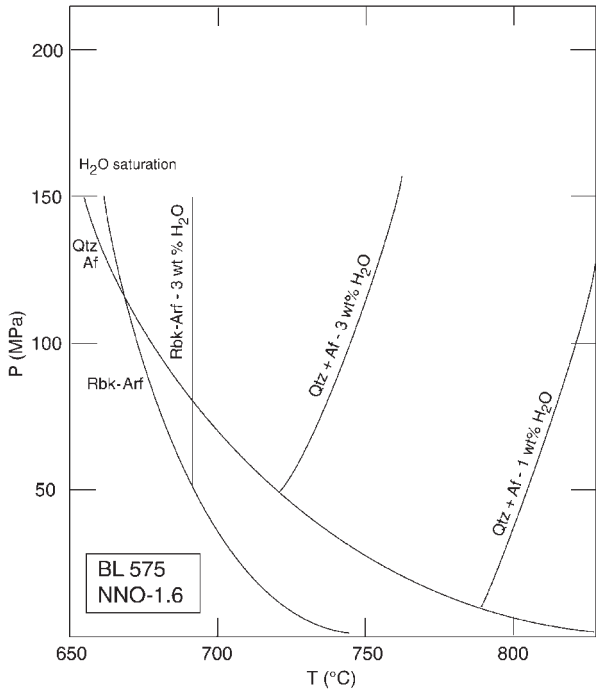

Fig. 6. *P–T* stability curves for quartz–alkali feldspar and riebeckite–arfvedsonite in BL 575 at H_2O saturation. The stability curves of quartz–alkali feldspar for a magma containing 1 and 3 wt % H_2O, and for riebeckite–arfvedsonite for 3 wt % H_2O, are also shown. The curves are labelled with minerals lying inside their respective stability fields.

to the H_2O-undersaturated character of the ascending magma. According to our data, ascent durations of <2 days are implied for a magma stored at 150 MPa, 830°C, with ~3 wt % H_2O, if quartz phenocrysts are to be preserved.

Pre-eruptive conditions at Naivasha

First-order constraints on pre-eruptive conditions can be made by direct comparison of the phase equilibria established here with the phase assemblages observed in the rocks. This assumes that, in the latter, bulk crystal–melt equilibrium prevailed shortly before eruption and was not subsequently altered during extrusion. The lack of conspicuous zoning of the major phases and of evidence for xenocrysts suggests that this is the case (Macdonald *et al.*, 1987).

Let us consider first ND 002 (Fig. 2). The absence of titanite indicates a pre-eruptive fO_2 close to or below FMQ. The stable coexistence of ferrohedenbergite and fayalite implies that pre-eruptive conditions were at the overlap in their stability fields. If the magma was at water saturation, then temperature is constrained by the liquidus of alkali feldspar, at ~700°C. Significantly lower temperatures are precluded by the hedenbergite-out reaction and by the appearance of quartz in the experiments. At 50 MPa coprecipitation of alkali feldspar, hedenbergite and magnetite (+ fayalite) is achieved at around 780°C at H_2O saturation (–2·5 wt % H_2O). Temperatures lower than 740°C are ruled out by quartz crystallization. On the other hand, lower melt water contents would require still higher temperatures. Melt water contents of melt inclusions in some Olkaria rocks reach 3·4 wt % (Wilding *et al.*, 1993), similar to those obtained here, whatever the pressure.

The presence of Na-amphibole at near-liquidus conditions in the natural BL 575 constrains the pre-eruptive temperature to have been lower than 700°C and, along with the absence of aegirine, suggests that the fO_2 was close to, or below, FMQ. Ignoring aenigmatite, the phase assemblage is restricted to a narrow *T*–melt water domain, with melt water contents of ~5·5 wt % and temperature below the intersection point of the biotite-in and Na-amphibole-in curves, which occurs slightly above 670°C. The estimate of melt water content is significantly higher than the maximum so far recorded in melt inclusions in quartz phenocrysts at Olkaria (Wilding *et al.*, 1993), which might indicate that 150 MPa for the pre-eruptive pressure of the storage zone is too high. A decrease in pressure would, nevertheless, not raise significantly the pre-eruption temperature estimate, as

this parameter is constrained by the occurrence of Na-amphibole whose stability is rather independent of pressure. However, a decrease in pressure removes amphibole from the liquidus (Fig. 6) and biotite has not been found at 50 MPa, both facts arguing against a pressure significantly lower than 150 MPa.

Sample SMN 49 lacks both aenigmatite and Na-amphibole as phenocrysts but has biotite, in addition to quartz and alkali feldspar. This implies a very restricted set of pre-eruptive temperatures and melt water contents, basically in the coldest and wettest part of the investigated domain, corresponding to the overlap between the stability fields of biotite, quartz and alkali feldspar but above that of Na-amphibole. At 150 MPa, a pre-eruptive temperature of 660°C and H_2O-saturated conditions are implied. Again, as for BL 575, considering the highest melt H_2O content found in melt inclusions (Wilding *et al.*, 1993), a pressure of 150 MPa would seem to be too high. At 50 MPa, coprecipitation of quartz and alkali feldspar is reached at 720°C at H_2O saturation ($\sim$3·3 wt % H_2O), but at this pressure and temperature biotite is not a liquidus phase.

Our experiments confirm the idea that peralkaline magmas may contain significant amounts of dissolved water, yet our estimates are nearly twice those from melt inclusion analyses (Wilding *et al.*, 1993). The phase equilibrium constraints detailed above are robust and we believe that this mismatch arises from a problem in interpreting the melt inclusion data. Such a difference could arise from a variety of factors, such as post-eruptive H_2O diffusive loss in the trapped melt inclusions or inclusion formation during ascent, i.e. at pressures lower than the pre-eruptive one, either of these processes being driven by, or occurring during, open-system degassing during eruption. Evidence for open-system degassing is in fact suggested by H/D isotope data (Wilding *et al.*, 1993). Restored pre-eruptive melt H_2O contents using measured δD and the matrix H_2O values of glassy volcanic rocks at Olkaria have yielded values up to 5·7 wt % (Wilding *et al.*, 1993), i.e. identical to the H_2O contents at saturation at 150 MPa and in agreement with our phase equilibrium constraints. We conclude that melt inclusion data at Olkaria provide only a minimum estimate of the amount of water present in the magma chamber before eruption.

In summary, the pre-eruptive intensive parameters derived in this study are characterized by last equilibration at an fO_2 at, or possibly below, FMQ, temperatures well below 800°C, and water-rich conditions. For the two more peralkaline samples, the pressure of the storage zone is probably >50 MPa, as indicated by the occurrence of near-liquidus biotite in the rocks. It cannot be much higher than 150 MPa, however, as increasing pressures will further depress the liquidus of tectosilicates, whereas that of amphibole will be correspondingly less affected, making it difficult to preserve the liquidus phase assemblage displayed by the rocks. Such a pressure for magma storage is also indicated by independent geochemical evidence (Davies & Macdonald, 1987).

ACKNOWLEDGEMENTS

Thorough and constructive reviews were provided by Mike Carroll, Gail Mahood and Jim Webster. Bernard W. Evans and Michel Pichavant provided useful comments. The very careful and constructive editorial handling of Dennis Geist is gratefully acknowledged.

REFERENCES

Abbott, R. N. (1981). AFM liquidus projections for granitic magmas, with special reference to hornblende, biotite and garnet. *Canadian Mineralogist* **19**, 103–110.

Bailey, D. K. (1974). Experimental petrology relating to oversaturated peralkaline volcanics: a review. *Bulletin of Volcanology* **38**, 635–652.

Bailey, D. K. & Cooper, J. P. (1978). Comparison of the crystallisation of pantelleritic obsidians under hydrous and anhydrous conditions. In: *Progress in Experimental Petrology*, *NERC Publications Series* **11**, 230–233.

Bailey, D. K. & Macdonald, R. (1970). Petrochemical variations among mildly peralkaline (comendite) obsidians from the ocean and continents. *Contributions to Mineralogy and Petrology* **28**, 340–351.

Bailey, D. K. & Macdonald, R. (1987). Dry peralkaline felsic liquids and carbon dioxide flux through the Kenya rift zone. In: Mysen, B. (ed.) *Magmatic Processes: Physicochemical Principles. Geochemical Society, Special Publication* **1**, 91–105.

Bailey, D. K. & Schairer, J. F. (1964). Feldspar–liquid equilibria in peralkaline liquids—the orthoclase effect. *American Journal of Science* **262**, 1198–1206.

Bailey, D. K. & Schairer, J. F. (1966). The system Na_2O–Al_2O_3–Fe_2O_3–SiO_2 at 1 atmosphere, and the petrogenesis of alkaline rocks. *Journal of Petrology* **7**, 114–170.

Bailey, D. K., Cooper, J. P. & Knight, J. L. (1974). Anhydrous melting and crystallisation of peralkaline obsidians. *Bulletin of Volcanology* **38**, 653–665.

Barberi, F., Santacroce, R. & Varet, J. (1974). Peralkaline rocks of the Afar depression. *Bulletin of Volcanology* **38**, 755–790.

Barberi, F., Ferrara, G., Santacroce, R., Treuil, M. & Varet, J. (1975). A transitional basalt–pantellerite sequence of fractional crystallisation, the Boina Centre (Afar, Ethiopia). *Journal of Petrology* **16**, 22–56.

Barclay, J., Carroll, M. R., Houghton, B. F. & Wilson, C. J. N. (1996). Pre-eruptive volatile content and degassing history of an evolving peralkaline volcano. *Journal of Volcanology and Geothermal Research* **74**, 75–87.

Bénard, F., Moutou, P. & Pichavant, M. (1985). Phase relations of tourmaline leucogranites and the significance of tourmaline in silicic magma. *Journal of Geology* **93**, 271–291.

Bizouard, H., Barberi, F. & Varet, J. (1980). Mineralogy and petrology of Erta Ale and Boina volcanic series, Afar rift, Ethiopia. *Journal of Petrology* **21**, 401–436.

Black, S., Macdonald, R. & Kelly, M. R. (1997). Crustal origin for peralkaline rhyolites from Kenya: evidence from U-series disequilibria and Th-isotopes. *Journal of Petrology* **38**, 277–297.

Blank, J., Stolper, E. & Carroll, M. R. (1993). Solubilities of carbon dioxide and water in rhyolitic melt at 850°C and 750 bars. *Earth and Planetary Science Letters* **119**, 27–36.

Bohrson, W. A. & Reid, M. R. (1997). Genesis of silicic peralkaline volcanic rocks in an ocean island setting by crustal melting and open-system processes: Socorro Island, Mexico. *Journal of Petrology* **38**, 1137–1166.

Bowen, N. L. (1937). Recent high temperature research on silicates and its significance in igneous geology. *American Journal of Science* **33**, 1–21.

Carmichael, I. S. E. (1962). Pantelleritic liquids and their phenocrysts. *Mineralogical Magazine* **33**, 86–113.

Carmichael, I. S. E. (1967). The iron–titanium oxides of salic volcanic rocks and their associated ferromagnesian silicates. *Contributions to Mineralogy and Petrology* **14**, 36–64.

Carmichael, I. S. E. (1991). The redox states of basic and silicic magmas: a reflection of their source regions? *Contributions to Mineralogy and Petrology* **106**, 129–141.

Carmichael, I. S. E. & MacKenzie, W. S. (1963). Feldspar–liquid equilibria in pantellerites: an experimental study. *American Journal of Science* **261**, 382–396.

Caroff, M., Maury, R. C., Leterrier, J., Joron, J. L., Cotten, J. & Guille, G. (1993). Trace element behavior in the alkali basalt–comenditic trachyte series from Mururoa atoll, French Polynesia. *Lithos* **30**, 1–22.

Civetta, L., D'Antonio, M., Orsi, G. & Tilton, G. R. (1998). The geochemistry of volcanic rocks from Pantelleria Island, Sicily channel: petrogenesis and characteristics of the mantle source region. *Journal of Petrology* **39**, 1453–1491.

Clarke, M. C. G., Woodhall, D. G., Allen, D. & Darling, G. (1990). Geological, volcanological and hydrogeological controls on the occurrence of geothermal activity in the area surrounding Lake Naivasha, Kenya. Report. Nairobi: Ministry of Energy, 138 pp.

Clemens, J. D. & Wall, V. J. (1981). Origin and crystallization of some peraluminous (S-type) granitic magmas. *Canadian Mineralogist* **19**, 111–131.

Clemens, J. D., Holloway, J. R. & White, A. J. R. (1986). Origin of an A-type granite: experimental constraints. *American Mineralogist* **71**, 317–324.

Conrad, W. K. (1984). The mineralogy and petrology of compositionally zoned ash flow tuffs, and related silicic volcanic rocks, from the McDermitt caldera complex, Nevada–Oregon. *Journal of Geophysical Research* **89**, 8639–8664.

Conrad, W. K., Nicholls, I. A. & Wall, V. J. (1988). Water-saturated and undersaturated melting of metaluminous and peraluminous crustal compositions at 10 kb: evidence for the origin of silicic magmas in the Taupo Volcanic Zone, New Zealand, and other occurrences. *Journal of Petrology* **29**, 765–803.

Crisp, J. A. & Spera, F. J. (1987). Pyroclastic flows and lavas of the Mogan and Fataga formations, Tejeda Volcano, Gran Canaria, Canary Islands: mineral chemistry, intensive parameters, and magma chamber evolution. *Contributions to Mineralogy and Petrology* **96**, 503–518.

Dall'Agnol, R., Scaillet, B. & Pichavant, M. (1999). An experimental study of a lower Proterozoic A-type granite from the eastern Amazonian craton, Brazil. *Journal of Petrology* **11**, 1673–1698.

Davies, G. R. & Macdonald, R. (1987). Crustal influences in the petrogenesis of the Naivasha basalt–comendite complex: combined trace element and Sr–Nd–Pb isotope constraints. *Journal of Petrology* **28**, 1009–1031.

Deer, W. A., Howie, R. A. & Zussman, J. (1978). *Rock Forming Minerals. Single-chain Silicates*. Harlow, UK: Longman, 668 pp.

Devine, J. D., Gardner, J. E., Brack, H. P., Layne, G. D. & Rutherford, M. J. (1995). Comparison of microanalytical methods for estimating H_2O contents of silicic volcanic glasses. *American Mineralogist* **80**, 319–328.

Ernst, W. G. (1962). Synthesis, stability relations and occurrence of riebeckite and riebeckite–arfvedsonite solid solutions. *Journal of Geology* **70**, 689–736.

Ewart, A., Taylor, S. R. & Capp, A. C. (1968). Geochemistry of the pantellerites of Mayor Island, New Zealand. *Contributions to Mineralogy and Petrology* **17**, 116–140.

Foerstner, H. (1881). Nota preliminare sulla geologia dell'isola di Pantelleria secondo gli studi fatti negli anni 1874 e 1881. *Bolletino di Rendi Conti Geologia Italia* **12**, 523–556.

Ghiorso, M. S. & Sack, R. O. (1991). Fe–Ti oxide geothermometry: thermodynamic formulation and the estimation of intensive variables in silicic magmas. *Contributions to Mineralogy and Petrology* **108**, 485–510.

Gibson, I. L. (1972). The chemistry and petrogenesis of a suite of pantellerites from the Ethiopian rift. *Journal of Petrology* **13**, 31–44.

Harris, C. (1983). The petrology of lavas and associated plutonic inclusions of Ascension island. *Journal of Petrology* **24**, 424–470.

Harris, C. (1986). A quantitative study of magmatic inclusions in the plutonic ejecta of Ascension island. *Journal of Petrology* **27**, 251–276.

Holloway, J. R. & Ford, C. E. (1975). Fluid absent melting of the fluorohydroxy-amphibole pargasite. *Earth and Planetary Science Letters* **25**, 44–48.

Holtz, F., Pichavant, M., Barbey, P. & Johannes, W. (1992). Effects of H_2O on liquidus phase relations in the haplogranite system at 2 and 5 kbar. *American Mineralogist* **77**, 1223–1241.

Johannes, W. & Holtz, F. (1996). *Petrogenesis and Experimental Petrology of Granitic Rocks*. Berlin: Springer, 335 pp.

Jørgensen, K. A. (1987). Mineralogy and petrology of alkaline granophyric xenoliths from the Thorsmork ignimbrite, southern Iceland. *Lithos* **20**, 153–168.

Kovalenko, V. I., Hervig, R. L. & Sheridan, M. F. (1988). Ion-microprobe analyses of trace elements in anorthoclase, hedenbergite, aenigmatite, quartz, apatite and glass in pantellerite: evidence for high water contents in pantellerite melts. *American Mineralogist* **73**, 1038–1045.

Kretz, R. (1983). Symbols for rock-forming minerals. *American Mineralogist* **68**, 277–279.

Lindsley, D. (1971). Synthesis and preliminary results on the stability of aenigmatite ($Na_2Fe_5TiSi_6O_{20}$). *Carnegie Institution of Washington, Annual Report Geophysical Laboratory* **1969–1970**, 188–190.

London, D., Morgan, G. B., VI & Hervig, R. V. (1989). Vapor-undersaturated experiments with Macusani glass + H_2O at 200 MPa, and the internal differentiation of granitic pegmatites. *Contributions to Mineralogy and Petrology* **102**, 1–17.

Lowenstern, J. B. & Mahood, G. A. (1991). New data on magmatic H_2O contents of pantellerites, with implications for petrogenesis and eruptive dynamics at Pantelleria. *Bulletin of Volcanology* **54**, 78–83.

Macdonald, R. (1974). Nomenclature and petrochemistry of the peralkaline oversaturated extrusive rocks. *Bulletin of Volcanology* **38**, 498–505.

Macdonald, R. & Bailey, D. K. (1973). The chemistry of the peralkaline oversaturated obsidians. *US Geological Survey, Professional Paper* **440-N**(Part 1), 1–37.

Macdonald, R., Davies, G. R., Bliss, C. M., Leat, P. T., Bailey, D. K. & Smith, R. L. (1987). Geochemistry of high-silicic peralkaline rhyolites, Naivasha, Kenya rift valley. *Journal of Petrology* **28**, 979–1008.

Macdonald, R., Kjarsgaard, B. A., Skilling, I. P., Davies, G. R., Hamilton, D. L. & Black, S. (1993). Liquid immiscibility between trachyte and carbonate in ash flow tuffs from Kenya. *Contributions to Mineralogy and Petrology* **114**, 276–287.

Mahood, G. A. (1981). Chemical evolution of a Pleistocene rhyolitic center: Sierra la Primavera, Jalisco, Mexico. *Contributions to Mineralogy and Petrology* **77**, 129–149.

Mahood, G. A. (1984). Pyroclastic rocks and calderas associated with strongly peralkaline magmatism. *Journal of Geophysical Research* **89**, 8540–8552.

Mahood, G. A., Halliday, A. N. & Hildreth, W. (1990). Isotopic evidence for the origin of pantellerites in a rift-related alkalic suite: Pantelleria, Italy. *IAVCEI Abstracts, International Volcanological Congress, Mainz*.

Manning, D. A. C. (1981). The effect of fluorine on liquidus phase relationships in the system Qz–Ab–Or with excess water at 1 kbar. *Contributions to Mineralogy and Petrology* **76**, 206–215.

Marshall, A. S., Hinton, R. W. & Macdonald, R. (1998). Phenocrystic fluorite in peralkaline rhyolites, Olkaria, Kenya rift valley. *Mineralogical Magazine* **62**, 477–486.

Martel, C., Pichavant, M., Bourdier, J. L., Traineau, H., Holtz, F. & Scaillet, B. (1998). Magma storage conditions and control of eruption regime in silicic volcanoes: experimental evidence from Mt. Pelée. *Earth and Planetary Science Letters* **156**, 89–99.

Martel, C., Pichavant, M., Holtz, F., Scaillet, B., Bourdier, J. L. & Traineau, H. (1999). Effects of fO_2 and H_2O on andesite phase relations between 2 and 4 kbar. *Journal of Geophysical Research* **104**, 29453–29470.

Mungall, J. E. & Martin, R. F. (1995). Petrogenesis of basalt–comendite and basalt–pantellerite suite, Terceira Azores, and some implications for the origin of ocean-island rhyolites. *Contributions to Mineralogy and Petrology* **119**, 43–55.

Nicholls, I. & Carmichael, I. S. E. (1969). Peralkaline acid liquids: a petrological study. *Contributions to Mineralogy and Petrology* **20**, 268–294.

Noble, D. C. (1968). Systematic variation of major element in comendite and pantellerite glasses. *Earth and Planetary Science Letters* **4**, 167–172.

Novak, S. W. & Mahood, G. A. (1986). Rise and fall of a basalt–trachyte–rhyolite magma system at the Kane Spring Wash caldera, Nevada. *Contributions to Mineralogy and Petrology* **94**, 352–373.

Pichavant, M. (1987). Effects of B and H_2O on liquidus phase relations in the haplogranite system at 1 kbar. *American Mineralogist* **72**, 1056–1070.

Pichavant, M. & Manning, D. A. C. (1984). Petrogenesis of tourmaline granites and topaz granites: the contribution of experimental data. *Physics of the Earth and Planetary Interiors* **35**, 31–50.

Pichavant, M., Boher, M., Stenger, J. F., Aissa, M. & Charoy, B. (1987). Relations de phases des granites de Beauvoir entre 1 et 3 kbar en conditions de saturation en H_2O. *Géologie France* **2–3**, 77–86.

Pownceby, M. I. & O'Neill, H. St C. (1994). Thermodynamic data from redox reactions at high temperatures. III. Activity–composition relations in Ni–Pd alloys from EMF measurements at 850–1250 K, and calibration of the NiO + Ni–Pd assemblage as a redox sensor. *Contributions to Mineralogy and Petrology* **116**, 327–339.

Robert, J. L. & Maury, R. (1979). Natural occurrence of an (Fe, Mn, Mg) tetrasilicic potassium mica. *Contributions to Mineralogy and Petrology* **68**, 117–123.

Roux, J. & Varet, J. (1975). Alkali–feldspar liquid equilibrium relationships in peralkaline oversaturated systems and volcanic rocks. *Contributions to Mineralogy and Petrology* **49**, 67–81.

Sato, H., Nakada, S., Fujii, T., Nakamura, M. & Suzuki-Kamata, K. (1999). Groundmass pargasite in the 1991–1995 dacite of Unzen volcano: phase stability experiments and volcanological implications. *Journal of Volcanology and Geothermal Research* **89**, 197–212.

Scaillet, B. & Evans, B. W. (1999). The June 15, 1991 eruption of Mount Pinatubo. I. Phase equilibria and pre-eruption P–T–fO_2–fH_2O conditions of the dacite magma. *Journal of Petrology* **40**, 381–411.

Scaillet, B., Pichavant, M., Roux, J., Humbert, G. & Lefèvre, A. (1992). Improvements of the Shaw membrane technique for measurement and control of fH_2 at high temperatures and pressures. *American Mineralogist* **77**, 647–655.

Scaillet, B., Pichavant, M. & Roux, J. (1995). Experimental crystallization of leucogranite magmas. *Journal of Petrology* **36**, 663–705.

Schairer, J. F. & Bowen, N. L. (1955). The system K_2O–Al_2O_3–SiO_2. *American Journal of Science* **253**, 681–746.

Schairer, J. F. & Bowen, N. L. (1956). The system Na_2O–Al_2O_3–SiO_2. *American Journal of Science* **254**, 129–195.

Schmidt, B. C., Scaillet, B. & Holtz, F. (1995). Accurate control of fH_2 in cold seal pressure vessels with the Shaw membrane technique. *European Journal of Mineralogy* **7**, 893–903.

Sutherland, D. S. (1974). Petrography and mineralogy of peralkaline silicic rocks. *Bulletin of Volcanology* **38**, 517–547.

Taylor, J. R., Wall, V. J. & Pownceby, M. I. (1992). The calibration and application of accurate redox sensors. *American Mineralogist* **77**, 284–295.

Thompson, R. N. & Chisholm, J. E. (1969). Synthesis of aenigmatite. *Mineralogical Magazine* **37**, 253–255.

Thompson, R. N. & MacKenzie, W. S. (1967). Feldspar–liquid equilibria in peralkaline acid liquids: an experimental study. *American Journal of Science* **265**, 714–734.

Tuttle, O. F. & Bowen, N. L. (1958). Origin of granite in the light of experimental studies in the system $NaAlSi_3O_8$–$KAlSi_3O_8$–SiO_2–H_2O. *Geological Society of America Memoir*, **74**, 153 pp.

Villari, L. (1974). The island of Pantelleria. *Bulletin of Volcanology* **38**, 680–724.

Washington, H. S. (1913). The volcanoes and rocks of Pantelleria: I. *Journal of Geology* **21**, 16–27.

Washington, H. S. (1914*a*). The volcanoes and rocks of Pantelleria: II. *Journal of Geology* **22**, 653–670.

Washington, H. S. (1914*b*). The volcanoes and rocks of Pantelleria: III. *Journal of Geology* **22**, 683–713.

Webster, J. D. (1992). Water solubility and chlorine partitioning in Cl-rich granitic systems. Effect of melt composition at 2 kbar and 800°C. *Geochimica et Cosmochimica Acta* **56**, 679–687.

Webster, J. D. (1997). Chloride solubility in felsic melts and the role of chloride in magmatic degassing. *Journal of Petrology* **38**, 1793–1807.

Webster, J. D., Holloway, J. R. & Hervig, R. L. (1987). Phase equilibria of a Be, U and F-enriched vitrophyre from Spor Mountain, Utah. *Geochimica et Cosmochimica Acta* **51**, 389–402.

Webster, J. D., Taylor, R. P. & Bean, C. (1993). Pre-eruptive melt composition and constraints on degassing of a water-rich pantellerite magma, Fantale volcano, Ethiopia. *Contributions to Mineralogy and Petrology* **114**, 53–62.

Weidner, J. R. & Martin, R. F. (1987). Phase equilibria of a fluorine rich leucogranite from the St. Austell pluton, Cornwall. *Geochimica et Cosmochimica Acta.* **51**, 1591–1597.

Wilding, M. C., Macdonald, R., Davies, J. R. & Fallick, A. E. (1993). Volatile characteristics of peralkaline rhyolites from Kenya: an ion microprobe, infrared spectroscopic and hydrogen isotope study. *Contributions to Mineralogy and Petrology* **144**, 264–275.

Wolff, J. A. & Wright, J. V. (1981). Formation of the Green Tuff, Pantelleria. *Bulletin of Volcanology* **44**, 681–690.

Wones, D. R. (1989). Significance of the assemblage titanite + magnetite + quartz in granitic rocks. *American Mineralogist* **74**, 744–749.

Wyllie, P. J. & Tuttle, O. F. (1961). Experimental investigation of silicate systems containing two volatile components: II—the effects of NH_3 and HF, in addition to H_2O, on the melting temperatures of albite and granite. *American Journal of Science* **259**, 128–143.

Zies, E. G. (1960). Chemical analyses of two pantellerites. *Journal of Petrology* **1**, 304–308.